



UNIVERSITY OF LEEDS

This is a repository copy of *Dynamic analysis of unsaturated porous media under moving loads by the time domain FEM using moving coordinates*.

White Rose Research Online URL for this paper:

<https://eprints.whiterose.ac.uk/218605/>

Version: Accepted Version

Article:

Pei, Y., Su, Q., Su, R. et al. (3 more authors) (2024) Dynamic analysis of unsaturated porous media under moving loads by the time domain FEM using moving coordinates. *Computers and Geotechnics*, 171. 106338. ISSN 0266-352X

<https://doi.org/10.1016/j.compgeo.2024.106338>

© 2024, Elsevier. This manuscript version is made available under the CC-BY-NC-ND 4.0 license <http://creativecommons.org/licenses/by-nc-nd/4.0/>. This is an author produced version of an article published in *Computers and Geotechnics*. Uploaded in accordance with the publisher's self-archiving policy.

Reuse

This article is distributed under the terms of the Creative Commons Attribution-NonCommercial-NoDerivs (CC BY-NC-ND) licence. This licence only allows you to download this work and share it with others as long as you credit the authors, but you can't change the article in any way or use it commercially. More information and the full terms of the licence here: <https://creativecommons.org/licenses/>

Takedown

If you consider content in White Rose Research Online to be in breach of UK law, please notify us by emailing eprints@whiterose.ac.uk including the URL of the record and the reason for the withdrawal request.



eprints@whiterose.ac.uk
<https://eprints.whiterose.ac.uk/>

1 **Dynamic analysis of unsaturated porous media under moving loads using a moving**
2 **coordinate approach**

3 Yanfei Pei^a, Qian Su^{a,b}, Rui Su^a, Kaiwen Liu^{a,b*}, David P. Connolly^c, Tengfei Wang^{a,b}

4 ^a School of Civil Engineering, Southwest Jiaotong University, Chengdu, Sichuan, China

5 ^b Key Laboratory of High-Speed Railway Engineering of Ministry of Education, Southwest Jiaotong University, Chengdu,
6 Sichuan, China

7 ^c School of Civil Engineering, University of Leeds, UK.

8 *Corresponding author, email: kaiwen.liu@queensu.ca

9
10

1 **Abstract**

2 Transport systems such as highways and railways are constructed on earthworks that experience fluctuating levels of
3 saturation. This can range from dry to fully saturated, however most commonly they are in a state of partial saturation. When
4 numerically modelling such problems, it is important to capture the response of the solid, liquid and gas phases in the material.
5 However, multi-physics solutions are computationally demanding and as a solution this paper presents a finite element
6 approach for the dynamic analysis of unsaturated porous media in a moving coordinate system. The first novelty of the work
7 is the development of a principle of relative motion for a three-phase medium, where the moving load is at rest while the
8 unsaturated porous medium moves relative to the load. This makes it particularly efficient for moving load problems such as
9 transport. The second novelty is a parametric investigation of the three-phase response of a partially saturated medium subject
10 to a moving load. The paper starts by presenting the time domain model in terms of its constitutive relationships and equations
11 for mass and momentum conservation. Next the model is validated using three case studies: the consolidation of a saturated
12 soil column, the dynamics of an unsaturated soil column and finally the response of a saturated foundation to a moving load.
13 It is then used to study a moving 2D plane strain load problem and its performance is compared to that of a standard FEM
14 solution which does not employ a moving coordinate system. Similar accuracy is obtained while computational efficiency is
15 improved by a factor of ten. Finally, the model is used to investigate the effect of degree of saturation and moving load speed
16 on the response of an unsaturated porous medium. It is found that both variables have a significant impact on the dynamic
17 response.

18 **Keywords:** Multi-physics modeling; Pore-water pressure; Unsaturated porous media; Moving loads; Highway-Railway
19 earthworks; Dynamic response
20

1 Introduction

2 Transport systems such as highways and railways are constructed on earthworks subject to varying levels of saturation. This can range from dry to fully saturated, however most commonly they are partially saturated, also known as being in an unsaturated condition. This degree of soil saturation can affect infrastructure performance by causing geotechnical problems such as erosion and subsidence (as shown in Figure 1). The occurrence of engineering problems resulting from unsaturated soil has become increasingly common in the construction of railway foundations (Indraratna [1], Yang [2], Fang [3]), highway foundations (Stormont and Zhou [4], Zornberg [5]), and airport runways Tang [6] in recent years.

3 Although a large number of studies have investigated the dynamic response of moving loads in dry soil conditions using the assumptions of traditional elastodynamics (e.g. Chumyem [7], Charoenwong [8]), they typically ignore the presence of liquid and gas phases. This is important because the dynamic response of unsaturated porous media differs significantly from that of elastic media (Fredlund and Rahardjo [9], Ng and Menzies [10]) due to the presence of pore water and gases (Ma [11]).

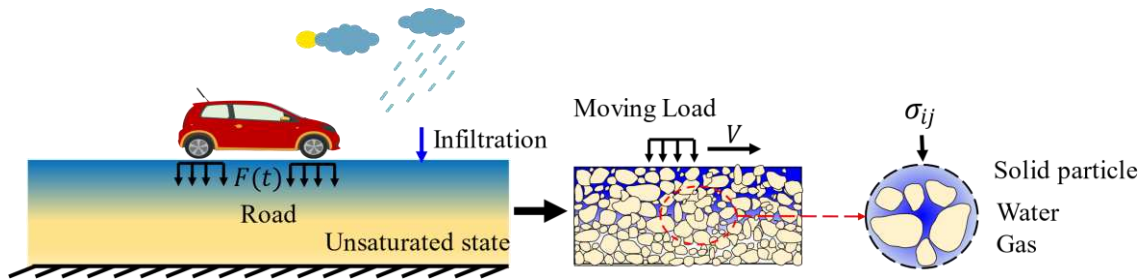


Figure 1 Unsaturated conditions in transportation geomaterials

4 In an attempt to include the effect of water in dynamic simulation models, fully saturated approaches were first proposed. The dynamic governing equation for saturated two-phase media in the fluid-solid coupling problem within porous media was initially established by Biot [12], before being expanded upon to incorporate anisotropy and viscoelasticity (Biot [13], Biot [14]). These developments were fundamental in describing the behavior of porous media. Zienkiewicz and Shiomi [15] proposed different coupling equations for saturated porous media, using various field variables such as $u - w$, $u - p$, and $u - U - p$ (where u is the displacement of the soil skeleton, w is the relative displacement of the fluid, U is the absolute displacement of the fluid, and p is the pore water pressure). These equations have been widely used in the field of geomechanics and are important for understanding the behavior of porous media. In parallel, Bowen [16] studied planar waves in two-phase saturated porous media using mixture theory.

5 In the field of geotechnical engineering, Prévost [17], Prevost [18] considered the non-linear behavior of the soil skeleton and established transient dynamic equations for saturated porous media. Once the governing equations were established, the study of solution methods became crucial for practical application. Therefore various analytical and numerical methods were proposed to solve these governing equations. For example, Simon [19] and Gajo and Mongiovi [20] proposed analytical approaches, which were accurate but limited to semi-infinite spaces and difficult to apply in cases with complex geometries, non-linear materials, and complicated boundary conditions. Meanwhile, because the governing equations are partial differential equations, obtaining analytical solutions under general initial and boundary conditions is challenging. Thus, numerical methods, particularly finite element methods, have been widely used, such as Ghaboussi and Wilson [21] and Zienkiewicz and Shiomi [15] who investigated saturated two-phase porous media. The theory of saturated two-phase porous media has since found numerous applications in engineering fields, such as the dynamic analysis of railway (Zhao [22]) and highway roadbeds (Liang and Liang [23]).

6 Fully saturated modeling is useful for transport problems where the infrastructure is subject to high levels of water (e.g. flooding). However, transport infrastructure is usually designed to divert water away as quickly as possible, for example through the use of super-elevations, well-designed drainage systems and elevated earthworks. Therefore, rather than being in a fully saturated state, it is more common for infrastructure to be in an unsaturated state. This requires a different modeling approach compared to those previously discussed.

The modeling of a three-phase unsaturated porous media requires more variables compared to a saturated porous media, owing to the presence of gas in the pores. For example, Thigpen and Berryman [24] presented a dynamic governing equation for a three-phase porous medium, which could be simplified to Biot's equation. Alternatively, Vardoulakis and Beskos [25] used mixture theory to formulate the dynamic equation for an unsaturated porous medium, which was compared to the governing equations of a saturated porous medium. Lu [26] proposed a frequency-wave number domain analytical approach to calculate the dynamic response of unsaturated foundations in a semi-infinite space. Similarly, Jiang and Ma [27], Tang [28], and Ye and Ai [29] employed analytical approaches to determine the dynamic response of unsaturated soil in a half-space. Although these analytical solutions are useful for understanding the general behavior of an unsaturated medium, their versatility is limited when dealing with problems that involve: intricate geometry, non-linearities, or non-standard boundary conditions. Instead, alternative approaches are required for these problems.

Although Finite Element Method (FEM) offers flexibility in modeling unsaturated porous media compared to analytical methods, its potential has not been widely explored for this application. Li [30] developed a finite element model for unsaturated porous media that considered the influence of temperature and four variables: $u - p - Sr - T$. Ghorbani [31], Ghorbani [32], Ghorbani [33] also proposed a finite element method that accounted for elastic-plastic deformation in unsaturated soils. However, these studies only explored the dynamic response of small unsaturated soil columns, leaving other potential applications unexplored.

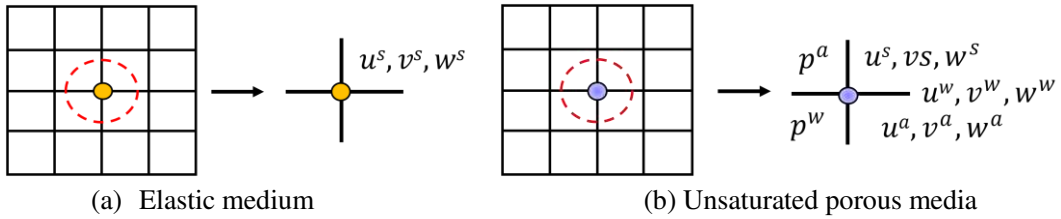


Figure 2 Node related variables for multi-physical field coupling problems (a) Elastic medium, (b) Unsaturated porous media (u^i, v^i, w^i are the three spatial components of solid, liquid, and gas displacement in unsaturated porous media, $i=s, w, a$)

A challenge with unsaturated modeling is that the solution of the extra nodal degree of freedom (Figure 2) requires significant additional computational effort. Therefore predicting the behavior of an unsaturated porous media with non-uniform geometry under a moving load requires an efficient numerical method. While the FEM is a widely used approach, capable of addressing geometric, material, and boundary nonlinearities, it suffers from reduced computational efficiency when applied to the dynamic response of unsaturated porous media under moving loads. This is because when solving with standard FEM, the location of the moving load changes constantly with time, thus requiring the dynamic matrix of the unsaturated porous media to be recomputed at each time instant. In order to meet solver stability criteria, a small step size is usually required, thus resulting in high computational time. Consequently, there is a need for more efficient computational techniques to overcome this limitation.

To address this, Wang [34], Wang [35] for example, proposed the Fourier finite element method (FFEM) to study the dynamic response of pavement structures under moving loads. Yang and Hung [36], Galvín [37], and Gao [38] and Charoenwong [39] also advanced the field of railway track dynamics through the use of 2.5D FEM. Liu [40], Liu [41], proposed a semi-analytical finite element method with Fourier transform in the direction of vehicle or moving load travel, while Shen [42] used sine and cosine Fourier series to depict the load and displacement along the longitudinal direction of the track. These methods all simplify the problem by removing the time and space dimensions in the moving load direction, thus reducing the calculation complexity for solving the dynamic response of structures under moving loads. Alternatively, Cao [43] introduced an alternative method using the Betti-Rayleigh Dynamic Reciprocal Theorem to simplify the analytical solution for structural vibration induced by moving loads.

In contrast to the aforementioned methods, the moving coordinate transformation uses a stationary load, while inducing

1 movement in its supporting structure. It can account for complex geometries and nonlinear material in the longitudinal
2 direction of the guideway, resulting in significant computational time savings. It has been widely used for analyzing the
3 dynamic response of both single-phase elastic media and saturated two-phase media. Krenk [44] first proposed using this
4 method for convective calculations to achieve fast computation. Subsequently, it found extensive application in solving
5 interaction problems between trains and tracks. For example, Koh [45] employed the moving element method to investigate
6 the vibration of track beams on viscoelastic foundations. Ang and Dai [46] also extended it to consider the dynamic response
7 analysis of viscoelastic foundations with non-uniform properties along the track direction. Tran [47] used it to analyze the
8 vertical dynamic response of high-speed railway structures under non-uniform motion. All these methods were employed
9 within the realm of single-phase elasticity. Recently, the application of this method has gradually expanded to two-phase
10 media (Liu [48] and Cao [49]).

11 Considering the challenges outlined above, this paper introduces a time domain FEM approach with moving coordinates
12 (M-FEM) as a way to efficiently calculate unsaturated porous media under moving loads. The M-FEM is based on the
13 principle of relative motion, which allows for the derivation of the dynamic governing equation of unsaturated porous media
14 using a moving coordinate system. The displacement coupled format $u^s - \bar{u}^w - \bar{u}^a$ (u^s is the displacement of the solid, \bar{u}^w
15 is the displacement of the liquid relative to the solid, \bar{u}^a is the displacement of the gas relative to the solid) is used to minimize
16 computational cost. To discretize the problem, the Galerkin method is used with three numerical examples to validate the
17 method. Also, a comparison of FEM and M-FEM calculations is provided in terms of computation cost and accuracy. In
18 addition, the M-FEM is used to evaluate the degree of saturation and moving load speed on the dynamic response of
19 unsaturated porous media.

20 **2 Methodology**

21 This section describes the calculation method for unsaturated porous media subject to moving loads. Firstly, the governing
22 equation describing the unsaturated porous media is established using coordinate transformation. Secondly, the governing
23 equation is discretized in space, including the establishment of a numerical stability method and boundary conditions. In the
24 third part, the *Generalized* α numerical integration method is used to discretize the governing equation in the time domain.

25 **2.1 Governing equations**

26 Numerical instability can occur in unsaturated simulations due to incompatibilities between the coupled physical variables
27 (Murad and Loula [50] and Li and Wei [51]). Therefore, this study proposes a displacement coupling scheme for the dynamic
28 governing equations of unsaturated porous media. Figure 3 illustrates this scheme, where v represents the load's velocity, and
29 $R = x - vt$ represents the horizontal axis in the moving coordinate system. Employing this scheme allows for the accurate
30 and consistent consideration of the physical properties of unsaturated porous media, leading to improved computational
31 efficiency while maintaining accuracy. The model is based on the diagram in Figure 3 below.

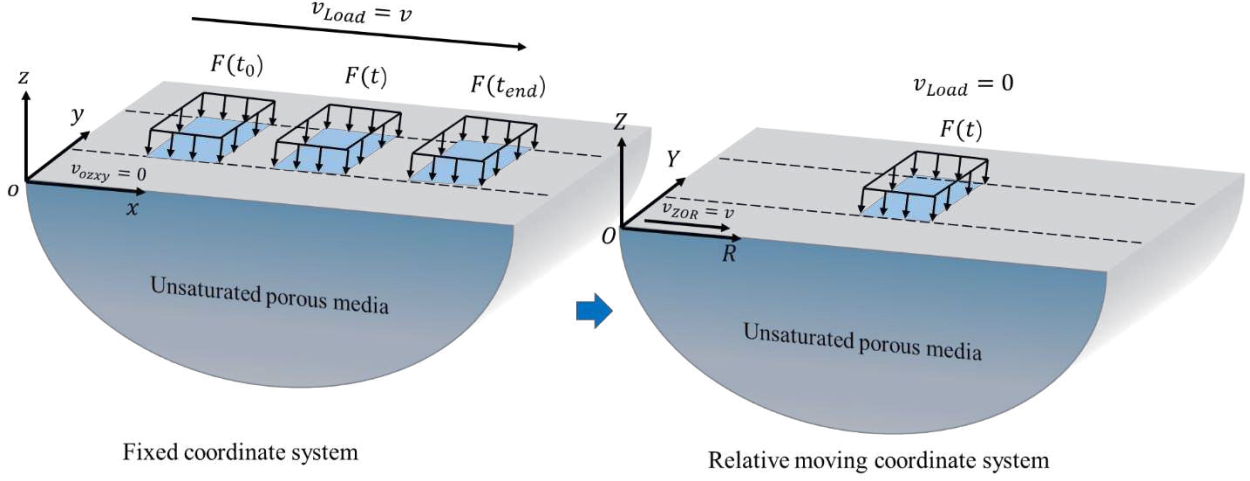


Figure 3 Moving coordinate relationships

In the fixed coordinate system $oxyz$ and moving coordinate system $ORYZ$, the relationship between variables is:

$$\begin{cases} \frac{\partial}{\partial x} = \frac{\partial}{\partial R}, \frac{\partial}{\partial x^2} = \frac{\partial}{\partial R^2} \\ \frac{\partial}{\partial t} \Big|_x = \frac{\partial}{\partial t} \Big|_R - v \frac{\partial}{\partial R} \\ \frac{\partial}{\partial t^2} \Big|_x = \frac{\partial}{\partial t^2} \Big|_R - 2v \frac{\partial}{\partial t \partial R} + v^2 \frac{\partial}{\partial R^2} \end{cases} \quad (1)$$

2.1.1 Constitutive relationship

According to the mixing theory proposed by Vardoulakis and Beskos [25], the total stress in an unsaturated porous medium can be expressed as:

$$\sigma_{ij} = (1 - n)\sigma_{ij}^s - nS_r p^w \delta_{ij} - n(1 - S_r)p^a \delta_{ij} \quad (2)$$

where n is porosity, S_r is the degree of saturation, p^w is pore water pressure, p^a is pore gas pressure.

Then, according to the effective stress principle proposed by Bishop and Blight [52], the total stress in unsaturated porous media can be expressed as:

$$\sigma_{ij} = 2\mu\epsilon_{ij} + \lambda\delta_{ij}e^s - \alpha\delta_{ij}p \quad (3)$$

Where $\alpha = 1 - \frac{K_b}{K_s}$ is the Biot coefficient, where K_b, K_s is the bulk compression modulus of the soil skeleton and soil particles. μ, λ are Lamé's parameters, e^s is the solid volumetric strain and ϵ_{ij} is the strain tensor.

2.1.2 Mass conservation

(a) Mass conservation of solids

According to the state equation for solids proposed by Tuncay and Corapcioglu [53], the equation between the rate of mass change and bulk compressibility modulus of the soil particles K_s is:

$$\frac{\partial \rho_s}{\rho_s \partial t} = -\frac{\partial \sigma_{ij}^s}{3K_s \partial t} \quad (4)$$

It is generally assumed the spatial gradient of n , and ρ_s is far lower than their time gradient (Tuncay and Corapcioglu [53]), meaning the spatial gradient change term can be omitted. Thus, the solid mass conservation equation is:

$$(1 - n) \frac{\partial \rho_s}{\partial t} - \rho_s \frac{\partial n}{\partial t} + \rho_s (1 - n) \nabla \cdot \mathbf{u}^s = 0 \quad (5)$$

The degree of saturation of an unsaturated porous media has an important effect on matric suction. Similarly, the mass conservation equation for the fluid is derived using a similar principle. Therefore, the relationship between matric suction and saturation is considered. Here, the V-G model proposed by Van Genuchten [54] is used to describe the soil-water characteristic curve (SWCC).

$$S_e = [1 + (\alpha_2 p)^d]^{-m} \quad (6)$$

$$S_e = (S_r - S_{w0}) / (1 - S_{w0}) \quad (7)$$

(b) Mass conservation of pore water

The mass conservation equation for the representative volume element of porous medium with respect to pore water is:

$$\frac{\partial(nS_r\rho_w)}{\partial t} + \nabla \cdot (nS_r\rho_w\dot{\mathbf{u}}^w) = 0 \quad (8)$$

where the relative displacement of pore water with respect to solids is, $\bar{\mathbf{u}}^w = nS_r(\dot{\mathbf{u}}^w - \dot{\mathbf{u}}^s)$. Mass conservation of pore water can then be reduced to the following form in a moving frame (see appendix for derivation):

$$w_1(\dot{p}^w - vp_{,R}^w) + w_2(\dot{p}^a - vp_{,R}^a) + \alpha S_r \nabla(\dot{u}_i^s - vu_{i,R}^s) + \nabla(\dot{u}_i^w - v\dot{u}_{i,R}^w) = 0 \quad (9)$$

(c) Mass conservation of pore air

The mass conservation equation for a representative volume element of the porous medium with respect to pore air is:

$$\frac{\partial[n\rho_a(1 - S_r)]}{\partial t} + \nabla \cdot [n(1 - S_r)\rho_a\dot{\mathbf{u}}^a] = 0 \quad (10)$$

The relative displacement of pore gas with respect to solids is defined as, $\bar{\mathbf{u}}^a = n(1 - S_r)(\dot{\mathbf{u}}^a - \dot{\mathbf{u}}^s)$. Mass conservation of pore air can then be reduced to the following form in a moving frame (see appendix for derivation):

$$g_1(\dot{p}^w - vp_{,R}^w) + g_2(\dot{p}^a - vp_{,R}^a) + \alpha(1 - S_r)\nabla(\dot{u}_i^s - vu_{i,R}^s) + \nabla(\dot{u}_i^a - v\dot{u}_{i,R}^a) = 0 \quad (11)$$

The equations for pore water pressure and pore air pressure respectively, obtained using (9) and (11) are (see appendix for derivation):

$$p^w = C_1^w \nabla \cdot \mathbf{u}^s + C_2^w \nabla \cdot \bar{\mathbf{u}}^w + C_3^w \nabla \cdot \bar{\mathbf{u}}^a \quad (12)$$

$$p^a = C_1^a \nabla \cdot \mathbf{u}^s + C_2^a \nabla \cdot \bar{\mathbf{u}}^w + C_3^a \nabla \cdot \bar{\mathbf{u}}^a \quad (13)$$

2.1.3 Momentum conservation

(a) Momentum conservation equation of mixture

According to Equation (3) and the law of momentum conservation, the momentum conservation of unsaturated porous media is:

$$\sigma_{ij,j} = \rho(\ddot{u}_i^s - 2v\dot{u}_{i,R}^s + v^2 u_{i,RR}^s) + \rho_w(\ddot{u}_i^w - 2v\dot{u}_{i,R}^w + v^2 \bar{u}_{i,RR}^w) + \rho_a(\ddot{u}_i^a - 2v\dot{u}_{i,R}^a + v^2 \bar{u}_{i,RR}^a) \quad (14)$$

Where ρ is mixed density, $\rho = (1 - n)\rho_s + nS_r\rho_w + n(1 - S_r)\rho_a$.

(b) Momentum conservation equation of pore water

Based on equation (12) and the law of momentum conservation, the momentum conservation equation of the pore water is:

$$C_1^w \nabla e^s + C_2^w \nabla e^w + C_3^w \nabla e^a + \rho_w(\dot{u}_i^s - 2v\dot{u}_{i,R}^s + v^2 u_{i,RR}^s) + \frac{\rho_w}{nS_r}(\ddot{u}_i^w - 2v\dot{u}_{i,R}^w + v^2 \bar{u}_{i,RR}^w) + \frac{\mu_w}{k_{rw}k}(\dot{u}_i^w - v\dot{u}_{i,R}^w) = 0 \quad (15)$$

Where k_{rw} is the relative permeability coefficient of the pore water, μ_w is the dynamic viscosity coefficient of the pore water and k is the intrinsic permeability of the unsaturated porous media.

(c) Momentum conservation equation of pore air

Based on equation (13) the momentum conservation equation of pore gas is:

$$C_1^a \nabla e^s + C_2^a \nabla e^w + C_3^a \nabla e^a + \rho_a(\dot{u}_i^s - 2v\dot{u}_{i,R}^s + v^2 u_{i,RR}^s) + \frac{\rho_a}{n(1 - S_r)}(\ddot{u}_i^a - 2v\dot{u}_{i,R}^a + v^2 \bar{u}_{i,RR}^a) + \frac{\mu_a}{k_{ra}k}(\dot{u}_i^a - v\dot{u}_{i,R}^a) = 0 \quad (16)$$

Where k_{ra} is the relative permeability coefficient of pore gas, μ_a is the dynamic viscosity coefficient of pore gas and k is the intrinsic permeability of the unsaturated porous media.

2.2 Spatial discretization

The Weighted Residual Method is applied to obtain the equivalent integral in a weak form for an unsaturated porous medium. The displacement of the solid is discretized as, $\mathbf{u}^s = \mathbf{N}_u \mathbf{u}$, the relative displacement of pore water is discretized as, $\bar{\mathbf{u}}^w = \mathbf{N}_w \bar{\mathbf{U}}_w$, and the relative displacement of pore gas is discretized as, $\bar{\mathbf{u}}^a = \mathbf{N}_a \bar{\mathbf{U}}_a$. Where $\mathbf{N}_u, \mathbf{N}_w, \mathbf{N}_a$ are the shape functions for the relative displacements of the solid, pore water and pore gas, respectively.

The momentum conservation equation of the mixture (14) is discrete and has the following form (see appendix for derivation):

$$\mathbf{M}_s \ddot{\mathbf{u}} + \mathbf{M}_{sw} \ddot{\bar{\mathbf{U}}}_w + \mathbf{M}_{sa} \ddot{\bar{\mathbf{U}}}_a + \mathbf{C}_s \dot{\mathbf{u}} + \mathbf{C}_{sw} \dot{\bar{\mathbf{U}}}_w + \mathbf{C}_{sa} \dot{\bar{\mathbf{U}}}_a + \mathbf{K}_s \mathbf{u} + \mathbf{K}_{sw} \bar{\mathbf{U}}_w + \mathbf{K}_{sa} \bar{\mathbf{U}}_a = \mathbf{f}^u \quad (17)$$

The momentum conservation equation of pore water (15) is discrete and has the following form:

$$\mathbf{M}_{ws} \dot{\mathbf{u}} + \mathbf{M}_{mw} \ddot{\bar{\mathbf{U}}}_w + \mathbf{C}_{mw}^s \dot{\mathbf{u}} + \mathbf{C}_{mw} \dot{\bar{\mathbf{U}}}_w + \mathbf{K}_{mw}^s \mathbf{u} + \mathbf{K}_{mw}^w \bar{\mathbf{U}}_w + \mathbf{K}_{mw}^a \bar{\mathbf{U}}_a = \mathbf{f}_{mw} \quad (18)$$

The momentum conservation equation of pore gas (16) is discrete and has the following form:

$$\mathbf{M}_{as} \dot{\mathbf{u}} + \mathbf{M}_{ma} \ddot{\bar{\mathbf{U}}}_a + \mathbf{C}_{ma}^s \dot{\mathbf{u}} + \mathbf{C}_{ma} \dot{\bar{\mathbf{U}}}_a + \mathbf{K}_{ma}^s \mathbf{u} + \mathbf{K}_{ma}^w \bar{\mathbf{U}}_w + \mathbf{K}_{ma}^a \bar{\mathbf{U}}_a = \mathbf{f}_{ma} \quad (19)$$

Through the above process, the analysis method for unsaturated porous media based on a moving coordinate system is established. Note that when the moving velocity of the load is 0 m/s ($v = 0$), the method simplifies to FEM.

2.2.1 Numerical stability

The traditional Galerkin method ($\bar{N}(x) = N(x)$) causes the governing equations to lose their original self-adjointness features due to the presence of the convection term ($2v\dot{\mathbf{u}}_{i,R}$). The existence of this term introduces negative numerical damping which may lead to numerical instability. This can be avoided by modifying the shape function, as per the theory of computational fluid dynamics. There are two common ways to solve this problem. Firstly, if using the Petrov-Galerkin variational principle, then the weight function requires the addition of asymmetric terms. Secondly, the approach proposed by Krenk [44] can be used. This uses the Taylor-Galerkin method to solve this problem, which is a Taylor series expansion of the term $2v\dot{\mathbf{u}}_{i,R}^s$. Comparing the two approaches, the Taylor-Galerkin method is relatively straightforward to implement because the compensation term can be added directly to the governing equation, which can still be discretized using the standard Galerkin method.

The Taylor-Galerkin method is therefore used in this paper to add artificial numerical damping to the governing equations. To do so, a convective term related to the second-derivative of space is added to the modified equation, so as to increase the damping of the whole dynamic system and eliminate any numerical oscillations caused by the negative numerical damping zone. This is described as:

$$\dot{\mathbf{u}}_{i,R} \approx -\frac{\Delta \dot{\mathbf{u}}_i}{h} + \frac{1}{2} h \ddot{\mathbf{u}}_{i,RR} \quad (20)$$

where h is the increment of ΔR in the opposite direction of the movement. The additional domain damping is:

$$\mathbf{C}_i^v = \int_{\Omega} \rho v h \mathbf{N}_{i,R}^T \mathbf{N}_{i,R} d\Omega \quad (21)$$

According to Krenk [44], the value of h is generally taken to be 0.3-0.4 times the size of the element in the R-direction.

2.2.2 Boundary conditions

The natural boundary conditions for pore pressures and stresses within the solution domain can be obtained through the equivalent integral in weak form. The natural boundary conditions are:

$$n_i (C_1^w \nabla \cdot \mathbf{u}^s + C_2^w \nabla \cdot \bar{\mathbf{u}}^w + C_3^w \nabla \cdot \bar{\mathbf{u}}^a) = p_n^w \quad (22)$$

$$n_i (C_1^a \nabla \cdot \mathbf{u}^s + C_2^a \nabla \cdot \bar{\mathbf{u}}^w + C_3^a \nabla \cdot \bar{\mathbf{u}}^a) = p_n^a \quad (23)$$

$$n_i (\sigma'_{ij} - \alpha S_r p^w - \alpha (1 - S_r) p^a) = t_i \quad (24)$$

Note that continuity is a requirement of the domain. Thus, the model should satisfy the displacement continuity conditions:

$$u = u_0 \quad (25)$$

$$\bar{u}^w = \bar{u}_0^w \quad (26)$$

$$\bar{u}^a = \bar{u}_0^a \quad (27)$$

2.3 Time integration

The *Generalized* α method was proposed by Chung and Hulbert [55] to solve dynamic problems. The method is similar to the Hilber-Hughes-Taylor (HHT) and Wood-Bossak-Zienkiewicz (WBZ) methods in that Newmark [56] is used for the calculation of velocity and displacement. Compared with HHT, WBZ, and *Newmark* β methods, this has been gradually applied to solve the strong nonlinear problem of multi-physical field coupling in porous media by providing a high frequency range adjustment (Erlicher [57], Kontoe [58]).

According to the results in Chapter 2.2, after forming the mass matrix, damping matrix and stiffness matrix, time-domain integration is used to solve the equations. The current displacement, velocity and acceleration of different physical fields are calculated according to the conditions at the previous timestep ($u_{n-1}, \dot{u}_{n-1}, \ddot{u}_{n-1}$). The displacement is of the form:

$$u = u_{n-1} + \Delta t \dot{u}_{n-1} + \frac{1}{2} \Delta t^2 \ddot{u} \quad (28)$$

The calculation formula for acceleration and velocity, obtained from (28), is:

$$\ddot{u} = \frac{2(u - u_{n-1} - \Delta t \dot{u}_{n-1})}{\Delta t^2} \quad (29)$$

$$\dot{u} = \dot{u}_{n-1} + \Delta t \ddot{u} \quad (30)$$

To reduce numerical oscillations, the General α time integration method uses the average form of acceleration $\ddot{u} = (1 - 2\beta)\ddot{u}_{n-1} + 2\beta\ddot{u}_n$ in place of the acceleration \ddot{u} , which is applied to (28) and (29) to obtain the modified form of displacement and acceleration.

$$u_n = u_{n-1} + \Delta t \dot{u}_{n-1} + \Delta t^2 \left[\left(\frac{1}{2} - \beta \right) \ddot{u}_{n-1} + \beta \ddot{u}_n \right] \quad (31)$$

$$\ddot{u}_n = \frac{(u_n - u_{n-1} - \Delta t \dot{u}_{n-1})}{\beta \Delta t^2} - \frac{1 - 2\beta}{2\beta} \ddot{u}_{n-1} \quad (32)$$

The acceleration term ($\ddot{u} = (1 - \gamma)\ddot{u}_{n-1} + \gamma\ddot{u}_n$) in the velocity formula is replaced resulting in:

$$\dot{u}_n = \dot{u}_{n-1} + \Delta t (1 - \gamma) \ddot{u}_{n-1} + \gamma \ddot{u}_n \quad (33)$$

A new format for calculating variables in time is obtained by introducing weight correction parameters based on the aforementioned discrete formats for displacement, velocity and acceleration. The displacement, velocity and acceleration in (17), (18) and (19) all adopt the weighted form proposed by Chung and Hulbert [55].

$$\ddot{u}_{n-\alpha_m} = (1 - \alpha_m) \ddot{u}_n + \alpha_m \ddot{u}_{n-1} \quad (34)$$

$$\dot{u}_{n-\alpha_f} = (1 - \alpha_f) \dot{u}_n + \alpha_f \dot{u}_{n-1} \quad (35)$$

$$u_{n-\alpha_f} = (1 - \alpha_f) u_n + \alpha_f u_{n-1} \quad (36)$$

$$t_{n-\alpha_f} = (1 - \alpha_f) t_n + \alpha_f t_{n-1} \quad (37)$$

(17), (18) and (19) take the following time integral form.

$$\mathbf{M} \ddot{u}_{n-\alpha_m} + \mathbf{C} \dot{u}_{n-\alpha_f} + \mathbf{K} u_{n-\alpha_f} = \mathbf{f}(t_{n-\alpha_f}) \quad (38)$$

$$\ddot{u}_0 = \mathbf{M}^{-1} [\mathbf{f}(0) - \mathbf{C} \dot{u}_0 - \mathbf{K} u_0] \quad (39)$$

The four parameters of the *Generalized* α method are: $\gamma = \frac{1}{2} - \alpha_m + \alpha_f$, $\beta = \frac{1}{4} (\gamma + \frac{1}{2})^2$, $\alpha_m = \frac{2\rho_\infty - 1}{1 + \rho_\infty}$, $\alpha_f = \frac{\rho_\infty}{1 + \rho_\infty}$. ρ_∞ is the high frequency factor, $\alpha_m, \alpha_f \leq 1$. The implementation process for the algorithm is provided in more detail in Ghorbani [31].

3 Validation

In order to verify the accuracy of the proposed numerical method for unsaturated porous media, three numerical examples are used. Example 1 is the analysis of dynamic consolidation of a saturated soil column. Example 2 is the analysis of the dynamic response of an unsaturated soil column. Example 3 is the analysis of the dynamic response of a saturated foundation under a moving load.

3.1 Validation 1: Saturated soil column consolidation

Liang and Liang [23] analyzed the dynamic response of saturated porous media using ABAQUS user-defined elements. This example uses the calculated parameters of the saturated soil column model proposed by Simon [59]. The input parameters of the saturated soil column are: $\rho_s = 0.3101\rho_s(\text{kg/m}^3)$, $\rho_w = 0.2977\rho_s(\text{kg/m}^3)$, $n=0.333$, $\mu_s = 1250\text{Pa}$, $\nu = 0.2$, $k_w = 1.4246\text{m/s}$, $\alpha = 0.667$ and $Q = 0.1385 \times 10^5\text{Pa}$ (Simon [59]). The width of the 2D model is 1.3164 m and the height is 31.5933m ($L \times H = 1.3164\text{m} \times 31.5933\text{m}$). The model is divided into 1 element in the horizontal direction and 600 elements in the vertical direction. The boundary conditions of the model are shown in Figure 4. The bottom of the saturated soil column is fixed and impermeable ($u_y^s = 0, \bar{u}_y^w = 0$). The left and right boundaries of the saturated soil column do not have transverse displacements and are impermeable ($u_x^s = 0, \bar{u}_x^w = 0$). Step loading ($F = F_{max}H(t)$) is applied to the top of the column: $F_{max} = 23750.5266\text{ N}$. The timestep is $\Delta t = \frac{T}{1000}$ and the total duration is 0.14942s.

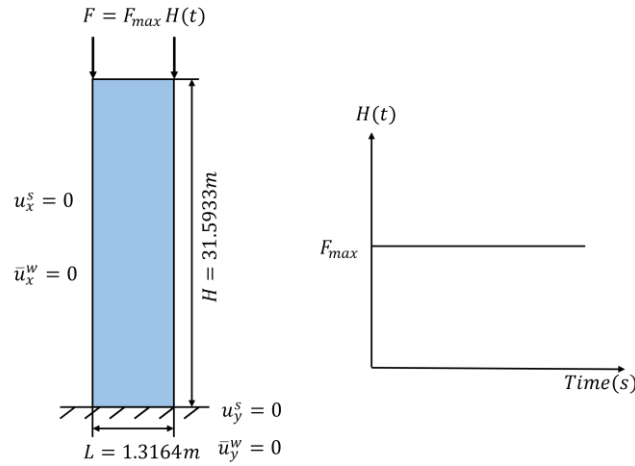
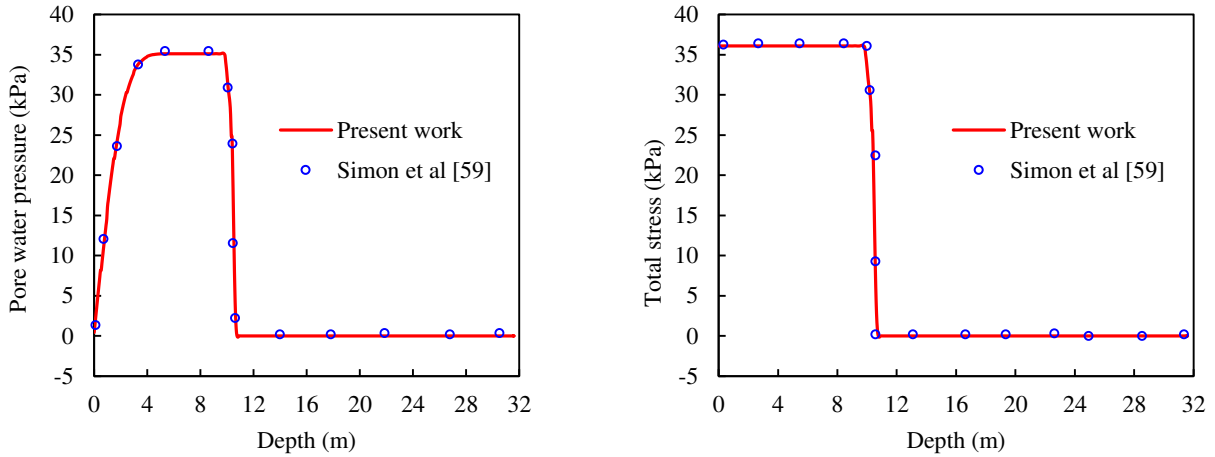


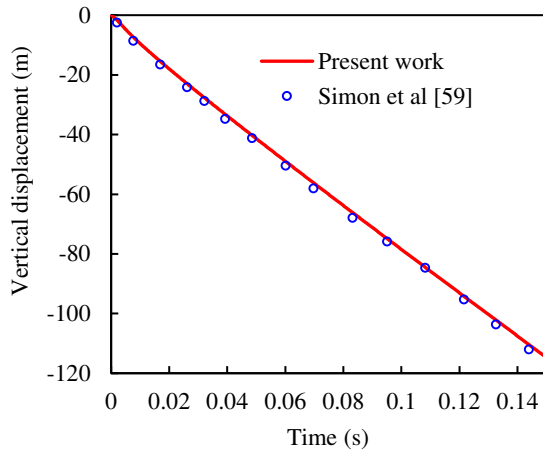
Figure 4 Saturated soil column validation case

The calculation parameters are $\nu = 0$, and $S_r = 0.99999$. Figure 5 shows the results of the proposed model are in good agreement with the results of Simon [59], indicating the accuracy of the proposed method for consolidation simulation.

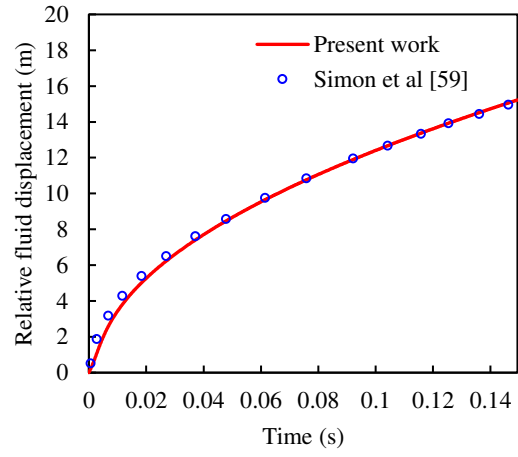


(a) Pore water pressure

(b) Total stress



(c) Vertical displacement



(d) Relative fluid displacement

Figure 5 Comparison of calculation results

3.2 Validation 2: Unsaturated soil column dynamics

In order to verify the accuracy of the proposed model for the dynamics of unsaturated porous media, an analytical approach of the 1D unsaturated soil column proposed by Li and Schanz [60] is used. The height of the unsaturated soil column is 10 m ($L=10$ m), the bottom of the column is impermeable and fixed, while the sides of the column are impermeable and rigid. A vertical load ($\sigma = 1.0Pa$) is applied instantaneously to the top of the soil column (Figure 6). The input parameters of the unsaturated soil column remain the same as those in Li and Schanz [60]: $n = 0.23$, $\rho_s = 2650kg/m^3$, $\rho_w = 997kg/m^3$, $\rho_a = 1.01kg/m^3$, $K = 1.02 \times 10^9Pa$, $G = 1.44 \times 10^9Pa$, $K_s = 3.5 \times 10^{10}Pa$, $K_w = 2.25 \times 10^9Pa$, $K_a = 1.10 \times 10^5Pa$, $k = 2.5 \times 10^{-12}m^2$. The Brooks and Corey model (Brooks [61]) was selected to define the soil-water characteristic curve of the unsaturated porous medium, with: $s = p^d S_e^{-1/d}$, $d = 1.5$. The model was divided into 500 elements and the initial solver timestep was 0.0001 s. The degree of saturation was $S_r = 0.9$. The model is calculated under plane strain conditions.

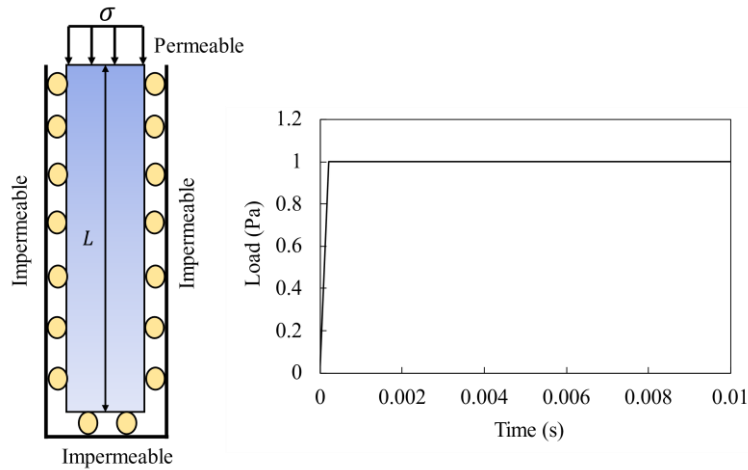
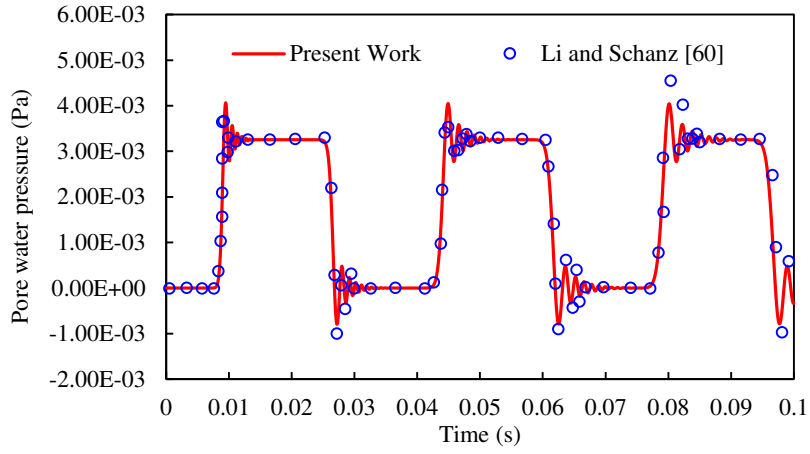
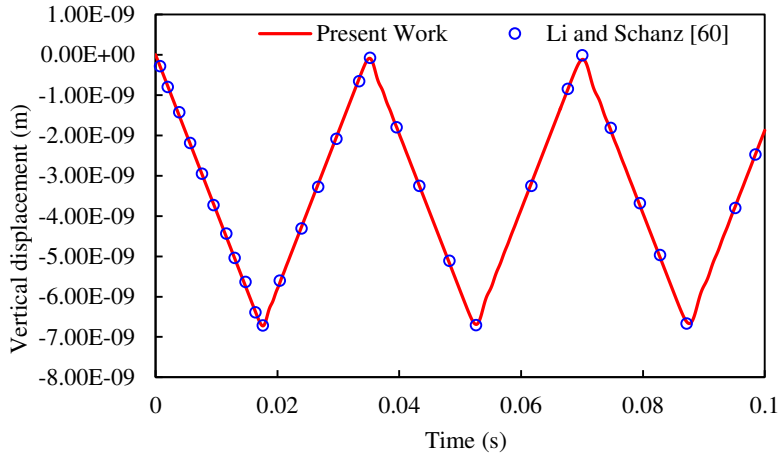


Figure 6 Unsaturated soil column validation case

The vertical displacement at the top of the soil column and the pore water pressure at the bottom of the soil column were compared with the analytical solutions proposed by Li and Schanz [60] (Figure 7). It can be observed that the proposed model yields results consistent with the analytical method, thus validating its accuracy for unsaturated dynamics problems.



(a) Pore water pressure at $S_r = 0.9$



(b) Vertical displacement at $S_r = 0.9$

Figure 7 Calculation results of unsaturated soil column

3.3 Validation 3: Saturated foundation with moving load

Finally, the case of a moving load on a saturated medium is studied. The computational parameters used for the validation are kept the same as Theodorakopoulos [62]. The depth and length of the domain are 18 m and 80 m respectively. The magnitude of the load is 0.4 MPa moving at a velocity of 100 m/s, as shown in Figure 8. The mesh size is 0.02 m in both horizontal and vertical directions, the initial timestep is 0.0001s and $S_r = 0.99999$. The model is calculated under plane strain conditions. The model is compared against the analytical solution proposed by Theodorakopoulos [62]. The left and right sides of the model limit lateral displacement and are impermeable, and the bottom boundary limits vertical displacement and is impermeable.

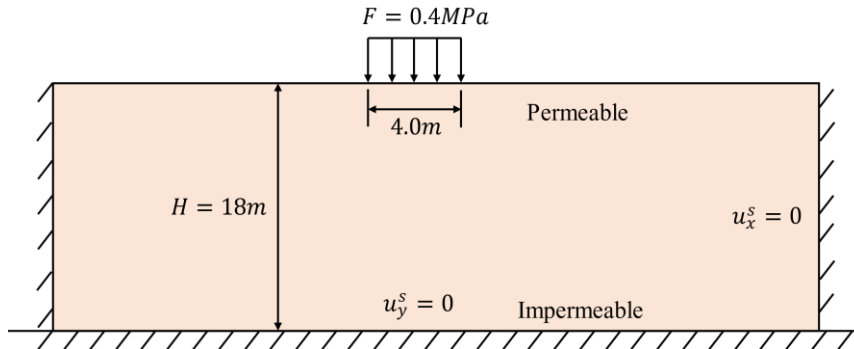
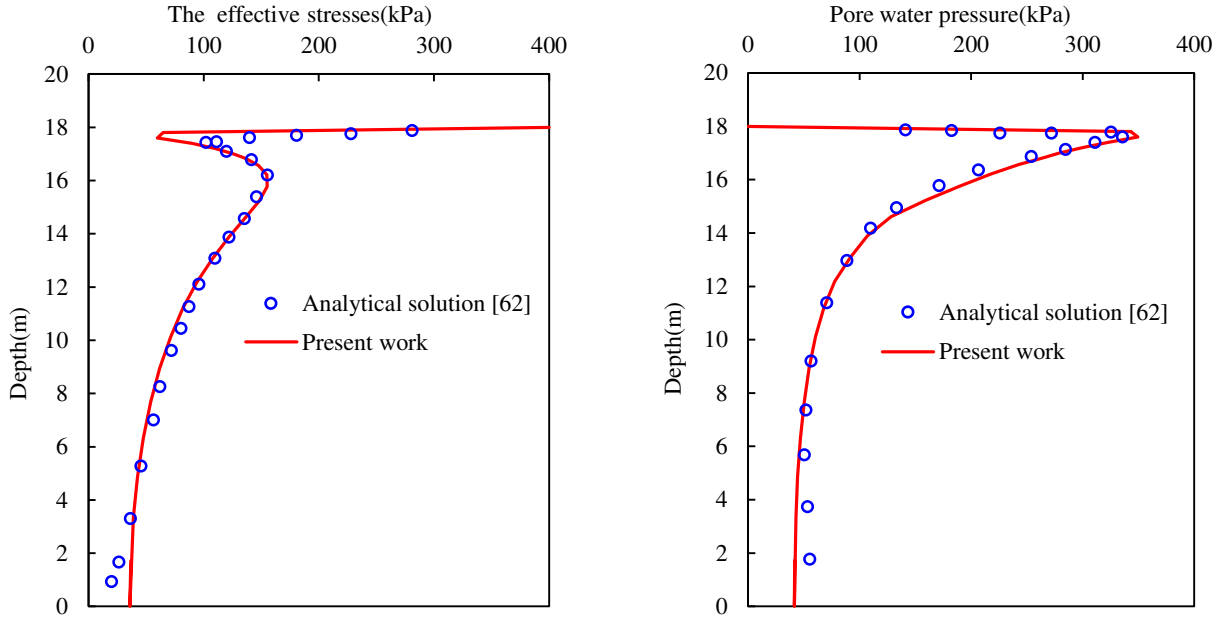


Figure 8 Moving load on saturated foundation validation case

A comparison of results is shown in Figure 9, where it is seen that the calculated results are in good agreement with the

analytical solution. This indicates the accuracy of proposed model for moving loads on saturated media.



(a) The effective stress

(b) Pore water pressure

Figure 9 Comparison of calculation results

4 Comparison between M-FEM and FEM

This section compares the results from the proposed M-FEM approach and standard FEM approach for moving loads on unsaturated porous media. The soil-water characteristics of the unsaturated porous medium are described and then the agreement between results and effort required for the FEM and M-FEM calculations are compared.

4.1 Characteristics of the unsaturated porous medium

An unsaturated porous medium with $S_r = 0.7$, length of 100 m and depth of 10 m is shown in Figure 10. The surface in contact with the moving load is the free seepage boundary. The load has a distribution length of 4 m, magnitude of $F = 0.7MPa$ and moved at a speed of $V = 0.4v_s$ (v_s is the shear wave velocity of the soil ($v_s = \sqrt{u_s/\rho_s}$)). The left and right sides of the model limit lateral displacement and are impermeable, and the bottom limits vertical displacement and is impermeable. The calculations are analysed in 2D conditions.

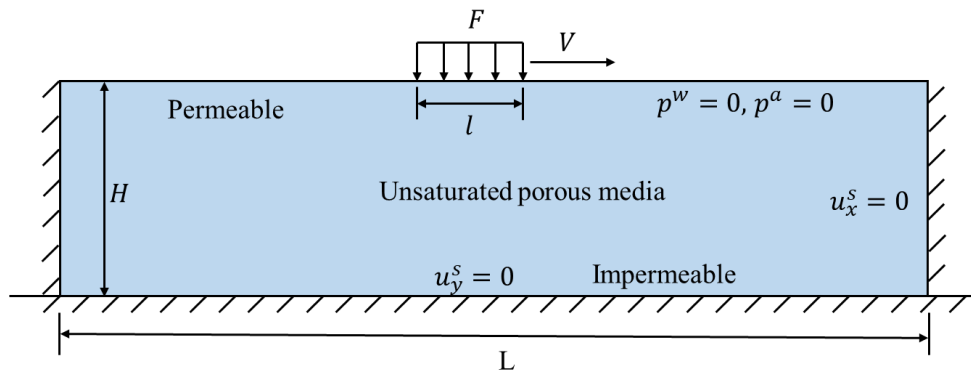


Figure 10 Computational modeling of unsaturated porous media

The hydraulic parameters of the unsaturated porous media are closely related to the degree of saturation. In order to investigate the dynamic response of the unsaturated porous media under moving load, the coupling relationship between the degree of saturation and matric suction, pore water and pore gas must be considered. The soil-water characteristic curve (Figure 11) describes these relationships, using parameters adopted from the literature, as shown in Table 1.

Table 1 Parameters defining the unsaturated porous medium Lo [63]

Parameters	Value
Shear modulus μ_s (MPa)	3.85
Solid density ρ_s (kg/m ³)	2650
Water density ρ_w (kg/m ³)	1000
Gas density ρ_a (kg/m ³)	1.29
Soil porosity n	0.45
Fitting parameter α_2	10^{-4}
Fitting parameter m	0.5
Fitting parameter d	2
Water viscosity μ_w (Pa · s)	0.001
Gas viscosity μ_a (Pa · s)	1.8×10^{-5}
Permeability k (m ²)	5.3×10^{-13}
Bulk modulus(K_s)(GPa)	35
Bulk modulus(K_w)(GPa)	2.25
Bulk modulus(K_a)(kPa)	145

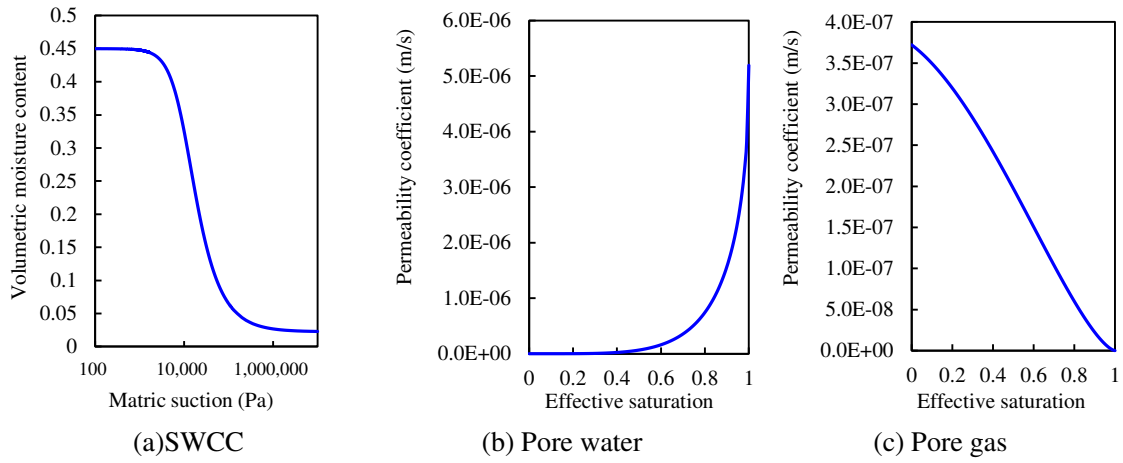


Figure 11 Hydraulic characteristics of the unsaturated porous medium

4.2 Calculation accuracy

This section compares the agreement between the results from the FEM and M-FEM approaches using the same computational material parameters (Table 1) and Lagrange first-order quadrilateral elements. The mesh size is 0.05m, the time step is 0.001s and the receivers are located directly below the centre of the moving load.

The differences between the models were quantified by analyzing pore water pressures, displacements and pore air pressures. From Figure 12, it is seen that the calculation trends and magnitudes agree well. Specifically, the maximum pore water pressure calculated with the FEM is 65.58 kPa and the maximum pore water pressure calculated with the M-FEM is 67.49 kPa, which is a difference of 2.91 %. The maximum displacements calculated using FEM and M-FEM are 0.372 m and 0.362 m respectively; a deviation of 3.04 %. The maximum pore gas pressure is 62.81 kPa and 64.63 kPa (2.9 %), calculated by FEM and M-FEM respectively. Thus, the calculations based on FEM and M-FEM show strong agreement.

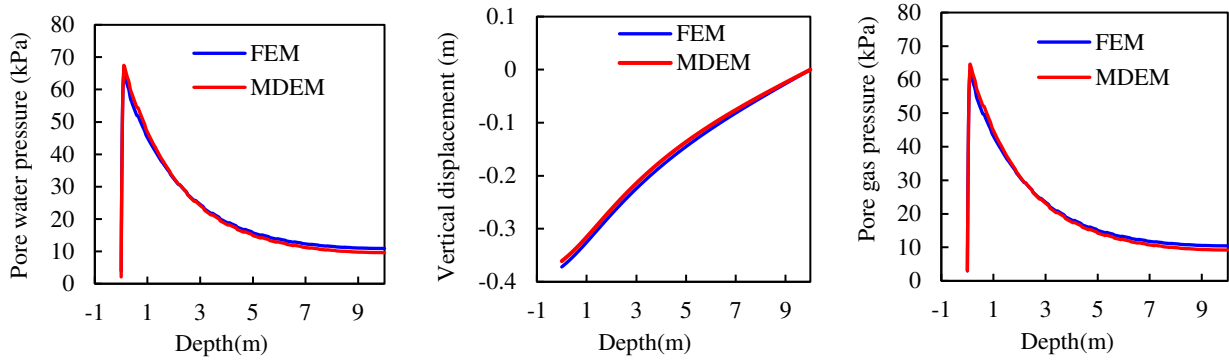


Figure 12 Comparison of M-FEM and FEM calculations

4.3 Computational efficiency comparison

The computational efficiency between FEM and M-FEM is compared, studying the simulations until the stabilization of all pore water pressures, gas pressures and vertical displacements. The factors of rectangular element sizes (0.2 m, 0.1 m and 0.05 m) and the different element orders (both Lagrange first-order and second-order elements) were considered. The processor is 13th Gen Intel(R) Core (TM) i9-13900K with 128GB of RAM. The computational model parameters and operating environment were identical and as discussed above.

For the Lagrange first-order elements, it can be seen from Figure 13 (a) that the computational efficiency for M-FEM is significantly better than that with FEM. The computation time with M-FEM is 9.3%, 9.1%, 9.0% of that with FEM, respectively for three different mesh sizes (0.2 m, 0.1 m and 0.05 m). Thus, the average time required with FEM is 10.94 times that with M-FEM. For the Lagrange second-order element (Figure 13 (b)), M-FEM also shows superior computational efficiency: the computation time for M-FEM is, 9.6%, 9.5%, 9.3% of that with FEM considering the three different mesh sizes (0.2 m, 0.1 m and 0.05 m respectively). Therefore the average computation time with FEM is 10.53 times that of M-FEM, which is similar to that for the case with first order elements.

The reason for this significantly higher efficiency is because M-FEM avoids the dynamic re-generation of the system matrix at each time step because it does not have to take into account the movement of the interaction points between the moving loads and the unsaturated porous medium with time. As a result, non-convergence is less of a concern meaning M-FEM can use larger time steps compared to FEM.

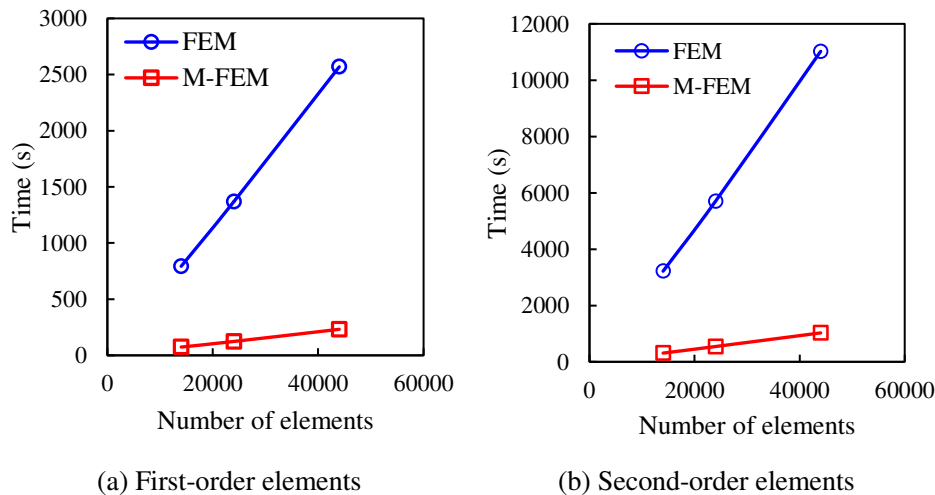
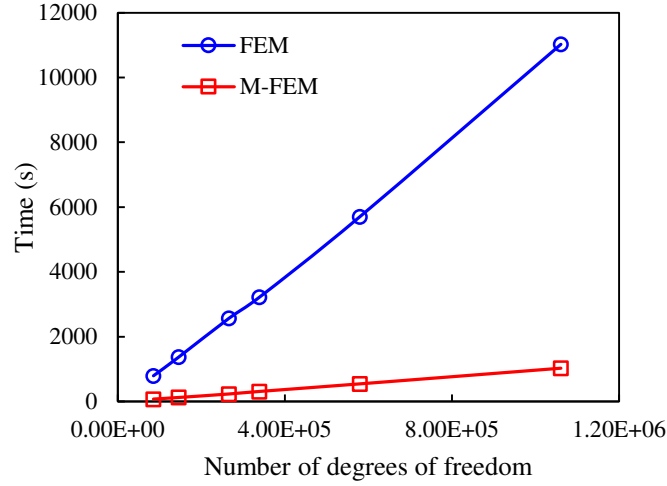


Figure 13 Calculation times for different orders of rectangular element

As shown in Figure 14, by analysing the number of degrees of freedom with computation time, it is seen that both FEM and M-FEM exhibit an approximately linear relationship. When the number of degrees of freedom of the model reaches 1,000,000, the computation time with FEM is approximately 3 hours, while it takes 0.28 hours with the M-FEM. This advantage of computational efficiency is particularly attractive for solving unsaturated engineering problems such as transport,

1 where there are often millions of degrees of freedom.

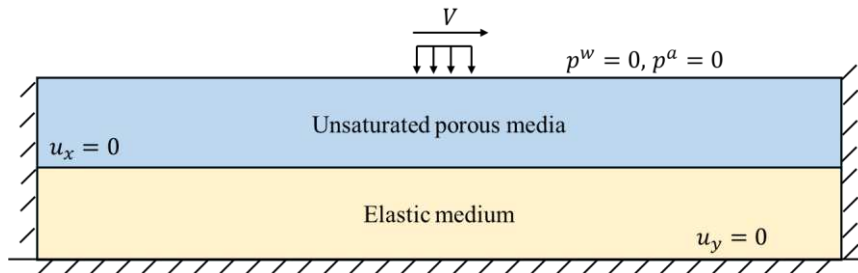


2
3 Figure 14 Calculation time for different degrees of freedom

4 **5 Unsaturated porous medium-elastic medium analysis**

5 This section explores the response of a 5 m-thick unsaturated porous layer overlaying a 5 m-thick layer of elastic (i.e. solid
6 only) layer, 100m long, as shown in Figure 15. The calculations are analysed in 2D conditions. This is intended to represent
7 a two-layered soil, where the top layer could be a clayey-sandy and the bottom layer an impermeable clay. The surface moving
8 load is 0.8MPa and the domain discretized using four-node Lagrangian elements with a mesh size of 0.1 m and time step of
9 0.001 s. The observation point of the dynamic response is set at the location directly below the moving load. The surface of
10 the upper unsaturated porous medium is permeable while the bottom boundary and sides are fixed. All input parameters for
11 the unsaturated porous medium are listed in Table 1 and the parameters for the elastic medium (modulus of elasticity, Poisson's
12 ratio and density are 48.6 MPa, 0.35, 1800kg/m³ respectively) are described in Wu [64].

13 The variables under consideration are the degree of saturation and moving load speed. Five values of degree of saturation
14 ($S_r = 0.2, 0.4, 0.6, 0.8, 0.95$) are considered, and five values of load speed related to the shear wave velocity of upper soil
15 ($V/v_s = 0.1, 0.3, 0.5, 0.7, 0.9$) are considered.



16
17 Figure 15 Unsaturated porous medium-elastic medium calculation example

18 **5.1 The effect of degree of saturation**

19 The gas phase in the pore space can affect wave transmission. If the presence of gas is not considered, the pore water
20 pressure in the pore space will be overestimated (Steeb [65], Wang [66], Zhang [67]). Therefore, simplifying an unsaturated
21 porous medium as a two-phase saturated medium will cause the calculation results to deviate significantly from the actual
22 state. Thus, it is worthwhile to study how the degree of saturation affects the dynamic response of unsaturated porous media.

23 (c) Displacement at depth

(d) Surface displacement

24 Figure 16 (a) shows that the pore water pressure increases rapidly and non-linearly as the degree of saturation increases.

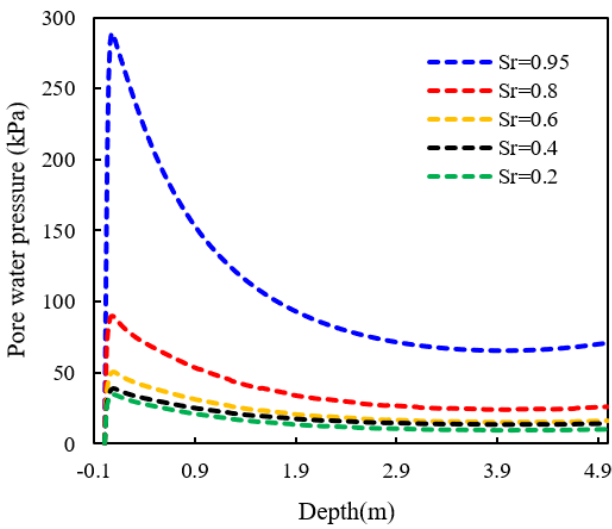
1 When S_r increases from 0.2 to 0.95, the maximum pore water pressure increases approximately 6.25 times. Further, when
 2 $S_r = 0.8$ increases to $S_r = 0.95$, this corresponds to the pore water pressure increasing by approximately 222%. (c)

3 Displacement at depth (d) Surface displacement

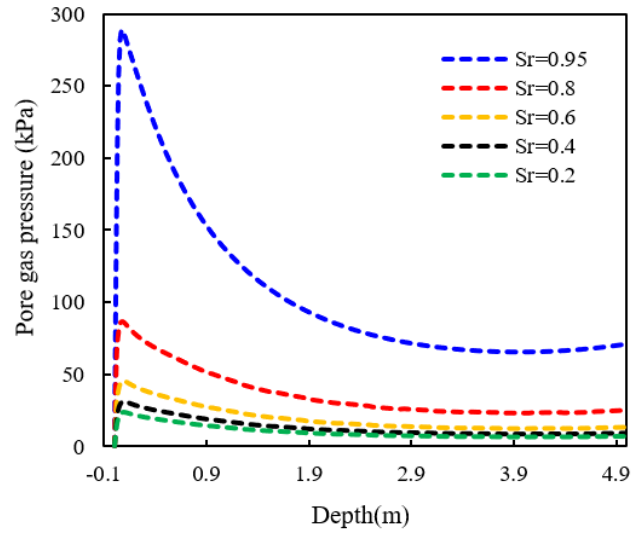
4 Figure 16 (b) shows that the variation in pore gas pressure with the degree of saturation is similar to the trend in pore water
 5 pressure. This shows that when the degree of saturation is greater than 0.8, the effect of matrix suction on gas and water
 6 pressures decreases as the porous medium gets close to being saturated. The values of pore gas pressure and pore water
 7 pressure will gradually become equal. (c) Displacement at depth (d) Surface displacement

8 Figure 16 (c) shows the relationship of vertical displacement versus different degrees of saturation. The pattern of vertical
 9 displacement decrease with depth is similar. The maximum and minimum displacements during the increase in the degree of
 10 saturation are 0.215 mm and 0.192 mm, respectively. (c) Displacement at depth (d) Surface
 11 displacement

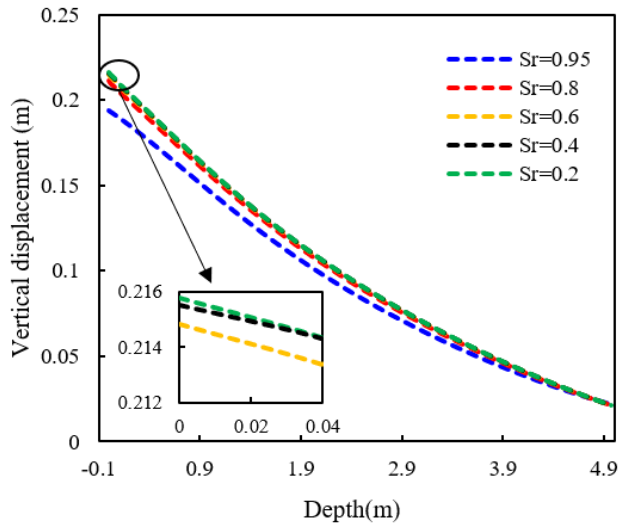
12 Figure 16 (d) represents the displacement distribution of the soil surface, when the degree of saturation is 0.2, 0.4 and 0.6.
 13 The difference in displacement is limited however when the degree of saturation is more than 0.6, the displacement
 14 distribution of the soil surface shows a more pronounced difference.



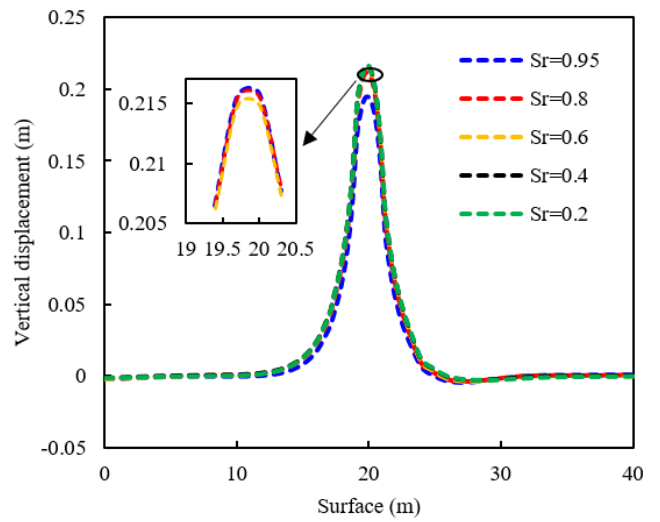
15 (a) Pore water pressure



16 (b) Pore gas pressure



(c) Displacement at depth



(d) Surface displacement

Figure 16 Effect of degree of saturation

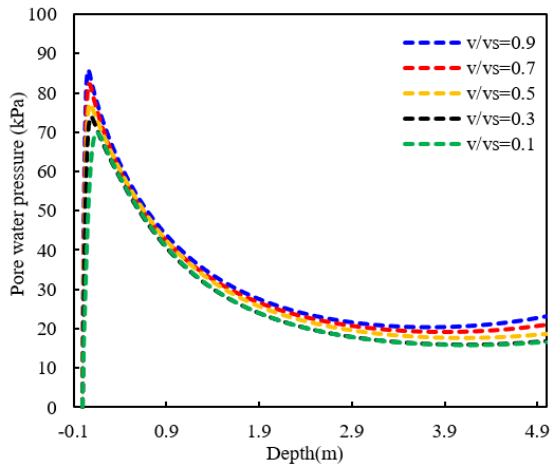
In unsaturated porous media, the percentage of water in the pores increases due to the increase in degree of saturation, which results in an increase in the compression modulus of the pores of the porous media (part of the water replaces the gas). As a result, the water and gas pressures within the pores increase. This increase occurs over the range of depths influenced by the load. As the degree of saturation increases, both pore water pressure and pore gas pressure escalate, leading to a reduction in the load borne by the soil skeleton. Consequently, the displacement resulting from effective stress decreases. Moreover, with an increase in the degree of saturation, the volume of water occupying the pores expands, resulting in a decrease in the number of compressible pores. Consequently, deformations of the porous medium skeleton diminish as saturation levels rise.

5.2 The effect of moving load velocity

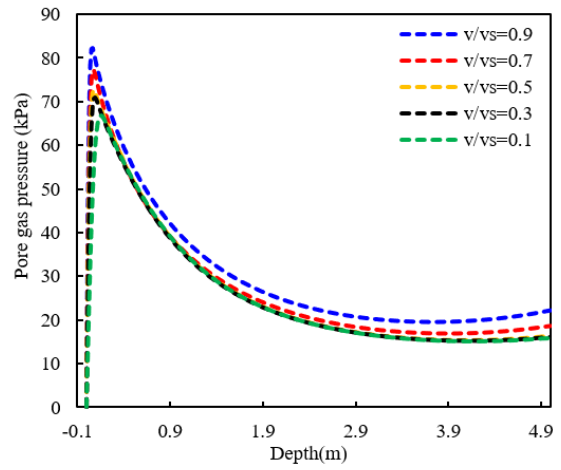
The velocity of a moving load affects the motion of water and gases in unsaturated porous media. In unsaturated porous media, the degree of interaction between fluid, gas and solid is different as the velocity of the moving load varies. Failure to consider the effect of the velocity on the unsaturated porous medium can result in an unreasonable design of structure (Cui [68]).

Figure 17 shows the effect of the moving load speeds on the pore water pressure, gas pressure and displacement located directly below the middle of moving load. The dynamic response indices (pore water pressure, pore gas pressure and displacement) all increase with an increase in speed. When the velocity of the moving load is increased from $v/v_s = 0.1$ to $v/v_s = 0.9$, the maximum pore water pressure, pore gas pressure and vertical displacement increase by 24.60%, 23.11%, and 26.01% respectively. Therefore moving speed can be an influential factor in the dynamic response of unsaturated porous media. Figure 17(d) shows the displacement distribution of the soil surface under different moving load speeds. When the moving load ratio exceeds 0.5, the moving load forms a clearer surface pattern on the soil surface, resulting in the bulging of certain soil sections.

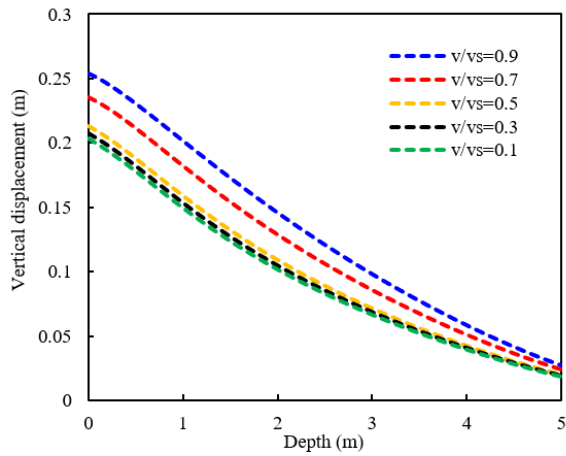
Inside the unsaturated porous medium, an increase in the velocity of the moving load can be equated to an increase in the loading frequency, which is because the width of the load is constant, and an increase in the velocity is equivalent to an increase in the loading frequency as explained by Cui [68]. Consequently, this intensifies the interactions among the solid, liquid, and gas phases within the unsaturated porous medium.



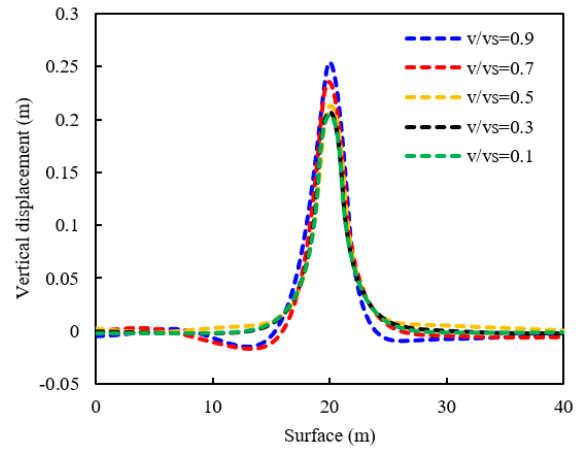
(a) Pore water pressure



(b) Pore gas pressure



(c) Displacement with depth



(d) Surface displacement

Figure 17 Effect of moving load velocity

6 Conclusions

This paper proposes a calculation approach for analyzing the dynamic response of unsaturated porous media subject to moving loads. The method combines a mass conservation equation, a momentum conservation equation, and a constitutive equation through a moving coordinate transformation to maximize computational efficiency. Spatial discretization is performed using the Galerkin-method, while time discretization is established using the General- α method. The validation of the proposed approach is performed by simulating three numerical examples from the published literature. The differences in calculation results between the proposed method and the FEM for a typical example are compared with respect to accuracy and computational time. Next, a numerical example is presented to illustrate the effect of the degree of saturation and moving load speed on the dynamic response of unsaturated porous media. Finally, new insights are provided into the dynamic response of unsaturated porous media. The main conclusions are:

(1) The M-FEM results show strong agreement FEM, but with significantly reduced computation time. Specifically, when comparing the computation time for either first-order or second-order elements, M-FEM requires approximately 1/10 of the time compared to the FEM. The computational time for FEM exhibits a nonlinear relationship with the number of degrees of freedom. Conversely, for the M-FEM approach, the number of degrees of freedom and the computational time have an approximately linear growth rate. This suggests M-FEM may offer a more efficient computational approach than traditional finite element methods, particularly for large domains.

(2) The dynamic response of unsaturated porous media is heavily influenced by its degree of saturation. As the degree of saturation increases, there is an increase in both pore water pressure and pore gas pressure. When the degree of saturation increases from 0.2 to 0.95, the maximum pore fluid pressure increases by a factor of 6.25. Additionally, the displacement of

1 unsaturated porous media decreases with increasing degree of saturation.

2 (3) As the moving load speed increases, the pore water pressure, pore gas pressure and displacement increase. For the
3 example considered, when the velocity of the moving load was increased from $v = 0.1v_s$ to $v = 0.9v_s$, the maximum pore
4 water pressure, the maximum pore air pressure and the maximum displacement increased by 24.60%, 23.11%, and 26.01%
5 respectively. The velocity of the moving load can have an amplifying effect on the dynamic response of unsaturated porous
6 media.

7 M-FEM shows good computational efficiency in 2D numerical examples, and it is predicted, based on the relationship
8 between the computational degrees of freedom and the computationally consumed time, that this method has potential in the
9 computation of complex unsaturated porous media.

10 **Acknowledgement**

11 The research was supported by National Natural Science Foundation of China (Grant No. 52078427 and 51978588);
12 Joint Fund for Basic Railway Research of China (Grant No. U2268213); The authors gratefully acknowledge their financial
13 support.
14
15

1 **Nomenclature**

2

3

Symbol	Physical significance
σ_{ij}	The total stress
σ_{ij}^s	The solid stress
p^w	Pore water pressure
p^a	Pore gas pressure
n	Porosity
S_r	The degree of saturation
δ_{ij}	Kronecker symbol
μ	Shear modulus
ϵ_{ij}	Strain tensor
λ	Lame parameters
e^s	Solid volumetric strain
α	Biot coefficient
p	Pore fluid pressure
K_b	Bulk compression modulus of soil skeleton
K_s	Bulk compression modulus of soil particle
S_e	The effective saturation
S_{w0}	The irreducible saturation
u^s	The displacement of solid
u^w	The displacement of pore water
u^a	The displacement of pore gas
ρ_s	The solid density
ρ_w	The density of pore water
ρ_a	The density of pore gas
ρ	The mixed density
k	The intrinsic permeability of the unsaturated porous media
k_{rw}	The relative permeability coefficient of pore water
μ_w	The dynamic viscosity coefficient of pore water
k_{ra}	The relative permeability coefficient of pore gas
μ_a	The dynamic viscosity coefficient of pore gas
\bar{u}^w	The relative displacement of pore water with respect to solids
\bar{u}^a	The relative displacement of pore gas with respect to solids
v	The speed of the moving load
∇	Gradient operator
t	Time
∂	The symbol for the derivative
L	The time change equation of saturation
α_2	Fitting parameter 1 of unsaturated porous medium
m	Fitting parameter 2 of unsaturated porous medium
d	Fitting parameter 3 of unsaturated porous medium
v_s	The shear wave velocity
M	The mass matrix
K	The stiffness matrix
C	The damping matrix
C_j^i	The intermediate variable
$\dot{\cdot}$	Rate of variable
$\ddot{\cdot}$	Acceleration of variable
N_u	The shape function of the solid displacement
N_w	The shape function for the relative displacement of pore water
N_a	The shape function for the relative displacement of pore gas
Ω	The field of integration
Γ	The integral boundary

1 Appendix

2 (1) Governing equation:

3 Substituting the total stress σ_{ij} into equations (2) and (3), the expression for solid stress (σ_{ij}^s) can be obtained as:

$$4 \quad \sigma_{ij}^s = \frac{1}{(1-n)} \{ \lambda \delta_{ij} e^s + 2\mu \epsilon_{ij} - [\alpha S_r - n S_r] \delta_{ij} p^w - [\alpha(1-S_r) - n(1-S_r)] \delta_{ij} p^a \}$$

5 Then, calculating the time derivative of σ_{ij}^s and substituting (4) into equation σ_{ij}^s , the equivalent expression of the rate of
6 change of soil mass can be obtained as:

$$7 \quad \frac{\partial \rho_s}{\rho_s \partial t} = \frac{-K_b \nabla \cdot \mathbf{u}^s + (\alpha S_r - n S_r) \frac{\partial p^w}{\partial t} + [\alpha(1-S_r) - n(1-S_r)] \frac{\partial p^a}{\partial t}}{(1-n)K_s}$$

8 The equivalent expression of the rate of change of soil mass is then substituted into the mass conservation equation for
9 solids to obtain the rate of change of porosity.

$$10 \quad \frac{\partial n}{\partial t} = \left(1 - n - \frac{K_b}{K_s}\right) \nabla \cdot \mathbf{u}^s + \frac{(\alpha S_r - n S_r)}{K_s} \frac{dp^w}{dt} + \frac{(\alpha(1-S_r) - n(1-S_r))}{K_s} \frac{dp^a}{dt}$$

11 The time derivative of saturation S_r is calculated according to (6) and (7), where S_e is the effective saturation and S_{w0} is
12 the irreducible saturation. The time change equation of saturation is then:

$$13 \quad \frac{dS_r}{dt} = -\alpha_2 m d \cdot (1 - S_{w0}) \cdot (S_e)^{\frac{m+1}{m}} \cdot \left(\left[(S_e)^{-\frac{1}{m}} - 1 \right]^{\frac{d-1}{d}} \right) \cdot \left(\frac{dp^a}{dt} - \frac{dp^w}{dt} \right)$$

14 Where $L = -\alpha_2 m d \cdot (1 - S_{w0}) \cdot (S_e)^{\frac{m+1}{m}} \cdot \left(\left[(S_e)^{-\frac{1}{m}} - 1 \right]^{\frac{d-1}{d}} \right)$.

15 The spatial gradient of n , ρ_w and S_r is significantly lower than its time gradient, meaning the mass conservation equation
16 of pore water is simplified as:

$$17 \quad n S_r \frac{\partial \rho_w}{\partial t} + S_r \rho_w \frac{\partial n}{\partial t} + n \rho_w \frac{\partial S_r}{\partial t} + n S_r \rho_w \nabla \cdot \mathbf{u}^w = 0$$

18 Combining the state equation of water and the rate of change of porosity and the time change equation of saturation, and
19 using the mass conservation equation for pore water, the following form is obtained:

$$20 \quad \left\{ n S_r \frac{1}{K_w} + \frac{S_r (\alpha S_r - n S_r)}{K_s} - n L \right\} \frac{\partial p^w}{\partial t} + \left\{ \frac{S_r [\alpha(1-S_r) - n(1-S_r)]}{K_s} + n L \right\} \frac{\partial p^a}{\partial t} \\ + \alpha S_r \nabla \cdot \mathbf{u}^s + n S_r (\nabla \cdot \mathbf{u}^w - \nabla \cdot \mathbf{u}^s) = 0$$

21 Again, the spatial gradient of n , ρ_a , S_r is much lower than their time derivatives, meaning the mass conservation of pore
22 air can be simplified to:

$$23 \quad n(1-S_r) \frac{\partial \rho_a}{\rho_a \partial t} + (1-S_r) \frac{\partial n}{\partial t} + n \frac{\partial(1-S_r)}{\partial t} + n(1-S_r) \nabla \cdot \mathbf{u}^a = 0$$

24 Combining the state equation for gas and the rate of change of porosity and the time change equation of saturation, and
25 bringing in the mass conservation equation for pore air, yields the following:

$$26 \quad \left[\frac{n(1-S_r)}{K_a} + (1-S_r) \frac{(\alpha(1-S_r) - n(1-S_r))}{K_s} - n L \right] \frac{\partial p^a}{\partial t} \\ 27 \quad + \left[(1-S_r) \frac{(\alpha S_r - n S_r)}{K_s} + n L \right] \frac{\partial p^w}{\partial t} + \alpha(1-S_r) \nabla \cdot \mathbf{u}^s + n(1-S_r) (\nabla \cdot \mathbf{u}^a - \nabla \cdot \mathbf{u}^s) = 0$$

28 The coefficients for each term in equations 12 and 13 are as follows:

1 where $C_1^w = \frac{\alpha(S_r g_2 - (1-S_r)w_2)}{(w_2 g_1 - w_1 g_2)}$, $C_2^w = \frac{g_2}{(w_2 g_1 - w_1 g_2)}$, $C_3^w = \frac{-w_2}{(w_2 g_1 - w_1 g_2)}$;

2 $C_1^a = \frac{\alpha(S_r g_1 - (1-S_r)w_1)}{(w_1 g_2 - w_2 g_1)}$, $C_2^a = \frac{g_1}{(w_1 g_2 - w_2 g_1)}$, $C_3^a = \frac{-w_1}{(w_1 g_2 - w_2 g_1)}$.

3 **(2) Spatial discretization**

4 The momentum conservation equation of the mix (14) is transformed into the weak form equivalent integral using the
5 Galerkin method:

6
$$\int_{\Omega} \{ \delta u_i 2\mu \epsilon_{ij,j} + \delta u_i [\lambda - \alpha S_r C_1^w - \alpha(1-S_r)C_1^a] \nabla e^s \delta_{ij} - \delta u_i \alpha [S_r C_2^w + (1-S_r)C_2^a] \nabla e^w \delta_{ij}$$

7
$$- \delta u_i \alpha [S_r C_3^w + (1-S_r)C_3^a] \nabla e^a \delta_{ij} \} d\Omega$$

8
$$= \int_{\Omega} (\rho \ddot{u}_i^s - 2\nu \rho \dot{u}_{i,R}^s + \rho v^2 u_{i,RR}^s) \delta u_i d\Omega + \int_{\Omega} (\rho_w \ddot{u}_i^w - 2\nu \rho_w \dot{u}_{i,R}^w + \rho_w v^2 \bar{u}_{i,RR}^w) \delta u_i d\Omega$$

9
$$+ \int_{\Omega} (\rho_a \ddot{u}_i^a - 2\nu \rho_a \dot{u}_{i,R}^a + \rho_a v^2 \bar{u}_{i,RR}^a) \delta u_i d\Omega$$

10 According to the Gauss-Green integral method, each term of the integral equation can be written in the following form:

11
$$\int_{\Omega} \delta u_i 2\mu \epsilon_{ij,j} d\Omega = - \int_{\Omega} \delta u_{i,j} 2\mu \epsilon_{ij} d\Omega + \int_{\Gamma} \delta u_i 2\mu \epsilon_{ij} d\Gamma$$

12
$$\int_{\Omega} \delta u_i [\lambda - \alpha S_r C_1^w - \alpha(1-S_r)C_1^a] \nabla e^s \delta_{ij} d\Omega$$

13
$$= - \int_{\Omega} \delta u_{i,j} [\lambda - \alpha S_r C_1^w - \alpha(1-S_r)C_1^a] e^s \delta_{ij} d\Omega + \int_{\Gamma} \delta u_i [\lambda - \alpha S_r C_1^w - \alpha(1-S_r)C_1^a] e^s \delta_{ij} d\Gamma$$

14
$$\int_{\Omega} -\delta u_i \alpha [S_r C_2^w + (1-S_r)C_2^a] \nabla e^w \delta_{ij} d\Omega$$

15
$$= \int_{\Omega} \delta u_{i,j} \alpha [S_r C_2^w + (1-S_r)C_2^a] e^w \delta_{ij} d\Omega - \int_{\Gamma} \delta u_i \alpha [S_r C_2^w + (1-S_r)C_2^a] e^w \delta_{ij} d\Gamma$$

16
$$\int_{\Omega} -\delta u_i \alpha [S_r C_3^w + (1-S_r)C_3^a] \nabla e^a \delta_{ij} d\Omega$$

17
$$= \int_{\Omega} \delta u_{i,j} \alpha [S_r C_3^w + (1-S_r)C_3^a] e^a \delta_{ij} d\Omega - \int_{\Gamma} \delta u_i \alpha [S_r C_3^w + (1-S_r)C_3^a] e^a \delta_{ij} d\Gamma$$

18
$$\int_{\Omega} \delta u_{i,j} 2\mu \epsilon_{ij} d\Omega + \int_{\Omega} \delta u_{i,j} [\lambda - \alpha S_r C_1^w - \alpha(1-S_r)C_1^a] e^s \delta_{ij} d\Omega - \int_{\Omega} \delta u_{i,j} \alpha [S_r C_2^w + (1-S_r)C_2^a] e^w \delta_{ij} d\Omega$$

19
$$- \int_{\Omega} \delta u_{i,j} \alpha [S_r C_3^w + (1-S_r)C_3^a] e^a \delta_{ij} d\Omega - \int_{\Gamma} \delta u_i 2\mu \epsilon_{ij} d\Gamma - \int_{\Gamma} \delta u_i [\lambda - \alpha S_r C_1^w - \alpha(1-S_r)C_1^a] e^s \delta_{ij} d\Gamma$$

20
$$+ \int_{\Gamma} \delta u_i \alpha [S_r C_2^w + (1-S_r)C_2^a] e^w \delta_{ij} d\Gamma + \int_{\Gamma} \delta u_i \alpha [S_r C_3^w + (1-S_r)C_3^a] e^a \delta_{ij} d\Gamma$$

21
$$+ \int_{\Omega} (\rho \ddot{u}_i^s - 2\nu \rho \dot{u}_{i,R}^s + \rho v^2 u_{i,RR}^s) \delta u_i d\Omega + \int_{\Omega} (\rho_w \ddot{u}_i^w - 2\nu \rho_w \dot{u}_{i,R}^w + \rho_w v^2 \bar{u}_{i,RR}^w) \delta u_i d\Omega$$

22
$$+ \int_{\Omega} (\rho_a \ddot{u}_i^a - 2\nu \rho_a \dot{u}_{i,R}^a + \rho_a v^2 \bar{u}_{i,RR}^a) \delta u_i d\Omega = 0$$

23
24 The mass, damping and stiffness matrices of (17) are:

25
$$\mathbf{M}_s = \rho \int_{\Omega} \mathbf{N}_u^T \mathbf{N}_u d\Omega, \quad \mathbf{M}_{sw} = \rho_w \int_{\Omega} \mathbf{N}_u^T \mathbf{N}_w d\Omega, \quad \mathbf{M}_{sa} = \rho_a \int_{\Omega} \mathbf{N}_u^T \mathbf{N}_a d\Omega$$

26
$$\mathbf{C}_s = -2\nu \rho \int_{\Omega} \mathbf{N}_u^T \mathbf{N}_{u,R} d\Omega, \quad \mathbf{C}_{sw} = -2\nu \rho_w \int_{\Omega} \mathbf{N}_u^T \mathbf{N}_{w,R} d\Omega, \quad \mathbf{C}_{sa} = -2\nu \rho_a \int_{\Omega} \mathbf{N}_u^T \mathbf{N}_{a,R} d\Omega$$

$$\begin{aligned}
1 \quad & \mathbf{K}_s = \rho v^2 \int_{\Omega} \mathbf{N}_{u,R}^T \mathbf{N}_{u,R} d\Omega + \int_{\Omega} \mathbf{B}_u^T \mathbf{D} \mathbf{B}_u d\Omega + (-\alpha s_r c_1^w - \alpha(1-s_r)c_1^a) \int_{\Omega} \mathbf{B}_u^T \mathbf{B}_u d\Omega, \\
2 \quad & \mathbf{K}_{sw} = \rho_w v^2 \int_{\Omega} \mathbf{N}_{u,R}^T \mathbf{N}_{w,R} d\Omega - \alpha [s_r c_2^w + (1-s_r)c_2^a] \int_{\Omega} \mathbf{B}_u^T \mathbf{B}_u^w d\Omega, \\
3 \quad & \mathbf{K}_{sa} = \rho_a v^2 \int_{\Omega} \mathbf{N}_{u,R}^T \mathbf{N}_{a,R} d\Omega - \alpha [s_r c_3^w + (1-s_r)c_3^a] \int_{\Omega} \mathbf{B}_u^T \mathbf{B}_u^a d\Omega, \quad \mathbf{f}^u = \int_{\Gamma} \mathbf{N}_u^T \mathbf{t}_u d\Gamma
\end{aligned}$$

4 The momentum conservation equation of pore water (15) is multiplied by the test function $\delta \bar{\mathbf{u}}^w$. Its equivalent integral, in
5 weak form, is obtained as:

$$\begin{aligned}
6 \quad & \int_{\Omega} \delta \bar{\mathbf{u}}_i^w (C_1^w \nabla \cdot \mathbf{u}^s + C_2^w \nabla \cdot \bar{\mathbf{u}}^w + C_3^w \nabla \cdot \bar{\mathbf{u}}^a) d\Omega - \int_{\Omega} \delta \bar{\mathbf{u}}^w \rho_w (\ddot{u}_i^s - 2v \dot{u}_{i,R}^s + v^2 u_{i,RR}^s) d\Omega \\
7 \quad & - \int_{\Omega} \delta \bar{\mathbf{u}}^w m_w (\ddot{u}_i^w - 2v \dot{u}_{i,R}^w + v^2 \bar{u}_{i,RR}^w) d\Omega - \int_{\Omega} \delta \bar{\mathbf{u}}^w b_w (\dot{u}_i^w - v \bar{u}_{i,R}^w) d\Omega \\
8 \quad & - \int_{\Gamma} \delta \bar{\mathbf{u}}^w n_i (C_1^w \nabla \cdot \mathbf{u}^s + C_2^w \nabla \cdot \bar{\mathbf{u}}^w + C_3^w \nabla \cdot \bar{\mathbf{u}}^a) d\Gamma = 0
\end{aligned}$$

9 The mass, damping and stiffness matrices of (18) are:

$$\begin{aligned}
10 \quad & \mathbf{M}_{ws} = -\rho_w \int_{\Omega} \mathbf{N}_w^T \mathbf{N}_u d\Omega, \quad \mathbf{M}_{mw} = -m_w \int_{\Omega} \mathbf{N}_w^T \mathbf{N}_w d\Omega, \\
11 \quad & \mathbf{C}_{mw}^s = 2v\rho_w \int_{\Omega} \mathbf{N}_w^T \mathbf{N}_{u,R} d\Omega, \quad \mathbf{C}_{mw} = 2vm_w \int_{\Omega} \mathbf{N}_w^T \mathbf{N}_{w,R} d\Omega - b_w \int_{\Omega} \mathbf{N}_w^T \mathbf{N}_w d\Omega, \\
12 \quad & \mathbf{K}_{mw}^s = -\rho_w v^2 \int_{\Omega} \mathbf{N}_{w,R}^T \mathbf{N}_{u,R} d\Omega + C_1^w \int_{\Omega} \nabla \mathbf{N}_w^T \nabla \mathbf{N}_u d\Omega, \\
13 \quad & \mathbf{K}_{mw}^w = -m_w v^2 \int_{\Omega} \mathbf{N}_{w,R}^T \mathbf{N}_{w,R} d\Omega + b_w v \int_{\Omega} \mathbf{N}_w^T \mathbf{N}_{w,R} + C_2^w \int_{\Omega} \nabla \mathbf{N}_w^T \nabla \mathbf{N}_w d\Omega, \\
14 \quad & \mathbf{K}_{mw}^a = C_3^w \int_{\Omega} \nabla \mathbf{N}_w^T \nabla \mathbf{N}_a d\Omega, \quad \mathbf{f}_{mw} = \int_{\Gamma} \mathbf{N}_w^T p_n^w d\Gamma
\end{aligned}$$

15 The momentum conservation equation for pore gas is multiplied by the trial function $\delta \bar{\mathbf{u}}^a$, and its equivalent integral, in
16 weak form, is obtained. Using the Gauss-Green integral method, it becomes:

$$\begin{aligned}
17 \quad & \int_{\Omega} \delta \bar{\mathbf{u}}_i^a (C_1^a \nabla \cdot \mathbf{u}^s + C_2^a \nabla \cdot \bar{\mathbf{u}}^w + C_3^a \nabla \cdot \bar{\mathbf{u}}^a) d\Omega - \int_{\Omega} \delta \bar{\mathbf{u}}^a \rho_a (\ddot{u}_i^s - 2v \dot{u}_{i,R}^s + v^2 u_{i,RR}^s) d\Omega \\
18 \quad & - \int_{\Omega} \delta \bar{\mathbf{u}}^a m_a (\ddot{u}_i^a - 2v \dot{u}_{i,R}^a + v^2 \bar{u}_{i,RR}^a) d\Omega - \int_{\Omega} \delta \bar{\mathbf{u}}^a b_a (\dot{u}_i^a - v \bar{u}_{i,R}^a) d\Omega \\
19 \quad & - \int_{\Gamma} \delta \bar{\mathbf{u}}^a n_i (C_1^a \nabla \cdot \mathbf{u}^s + C_2^a \nabla \cdot \bar{\mathbf{u}}^w + C_3^a \nabla \cdot \bar{\mathbf{u}}^a) d\Gamma = 0
\end{aligned}$$

20 The mass, damping and stiffness matrices of (19) are:

$$\begin{aligned}
21 \quad & \mathbf{M}_{as} = -\rho_a \int_{\Omega} \mathbf{N}_a^T \mathbf{N}_u d\Omega, \quad \mathbf{M}_{ma} = -m_a \int_{\Omega} \mathbf{N}_a^T \mathbf{N}_a d\Omega, \\
22 \quad & \mathbf{C}_{ma}^s = 2v\rho_a \int_{\Omega} \mathbf{N}_a^T \mathbf{N}_{u,R} d\Omega, \quad \mathbf{C}_{ma} = 2vm_a \int_{\Omega} \mathbf{N}_a^T \mathbf{N}_{a,R} d\Omega - b_a \int_{\Omega} \mathbf{N}_a^T \mathbf{N}_a d\Omega, \\
23 \quad & \mathbf{K}_{ma}^s = -\rho_a v^2 \int_{\Omega} \mathbf{N}_{a,R}^T \mathbf{N}_{u,R} d\Omega + C_1^a \int_{\Omega} \nabla \mathbf{N}_a^T \nabla \mathbf{N}_u d\Omega, \quad \mathbf{K}_{ma}^w = C_2^a \int_{\Omega} \nabla \mathbf{N}_a^T \nabla \mathbf{N}_w d\Omega, \\
24 \quad & \mathbf{K}_{ma}^a = -m_a v^2 \int_{\Omega} \mathbf{N}_{a,R}^T \mathbf{N}_{a,R} d\Omega + b_a v \int_{\Omega} \mathbf{N}_a^T \mathbf{N}_{a,R} + C_3^a \int_{\Omega} \nabla \mathbf{N}_a^T \nabla \mathbf{N}_a d\Omega, \\
25 \quad & \mathbf{f}_{ma} = \int_{\Gamma} \mathbf{N}_a^T p_n^a d\Gamma.
\end{aligned}$$

26
27

Reference

- [1] Indraratna, B., Salim, W., Rujikiatkamjorn, C. Advanced rail geotechnology-ballasted track: CRC press, 2011.
- [2] Yang, S.-R., Lin, H.-D., Kung, J.H., Huang, W.-H., 2008. Suction-controlled laboratory test on resilient modulus of unsaturated compacted subgrade soils. *J. Geotech. Geoenviron. Eng.* 134 (9), 1375-84.
- [3] Fang, R., Lu, Z., Yao, H., Luo, X., Yang, M., 2018. Study on dynamic responses of unsaturated railway subgrade subjected to moving train load. *Soil Dyn. Earthquake Eng.* 115 319-23.
- [4] Stormont, J.C., Zhou, S., 2005. Impact of unsaturated flow on pavement edgedrain performance. *J. Transp. Eng.* 131 (1), 46-53.
- [5] Zornberg, J.G., Azevedo, M., Sikkema, M., Odgers, B., 2017. Geosynthetics with enhanced lateral drainage capabilities in roadway systems. *Transp. Geotech.* 12 85-100.
- [6] Tang, C., Lu, Z., Yao, H., Guo, S., Han, Y., 2021. Vibration characteristics of unsaturated runways under moving aircraft loads. *Int. J. Struct. Stab. Dyn.* 21 (05), 2150065.
- [7] Chumyen, P., Connolly, D., Woodward, P., Markine, V., 2022. The effect of soil improvement and auxiliary rails at railway track transition zones. *Soil Dyn. Earthquake Eng.* 155 107200.
- [8] Charoenwong, C., Connolly, D., Woodward, P., Galvín, P., Costa, P.A., 2022. Analytical forecasting of long-term railway track settlement. *Comput. Geotech.* 143 104601.
- [9] Fredlund, D.G., Rahardjo, H. Soil mechanics for unsaturated soils: John Wiley & Sons, 1993.
- [10] Ng, C.W.W., Menzies, B. Advanced unsaturated soil mechanics and engineering: CRC Press, 2014.
- [11] Ma, Q., Shu, J., Zhou, F., 2022. Theoretical study of S wave passing through a double-layer wave impeding block in the unsaturated soil. *Comput. Geotech.* 152 105018.
- [12] Biot, M.A., 1941. General theory of three - dimensional consolidation. *J. Appl. Phys.* 12 (2), 155-64.
- [13] Biot, M.A., 1956. Theory of propagation of elastic waves in a fluid - saturated porous solid. II. Higher frequency range. *The Journal of the acoustical Society of america.* 28 (2), 179-91.
- [14] Biot, M.A., 1962. Generalized theory of acoustic propagation in porous dissipative media. *The Journal of the Acoustical Society of America.* 34 (9A), 1254-64.
- [15] Zienkiewicz, O., Shiomi, T., 1984. Dynamic behaviour of saturated porous media; the generalized Biot formulation and its numerical solution. *Int. J. Numer. Anal. Methods Geomech.* 8 (1), 71-96.
- [16] Bowen, R.M., 1979. A theory of constrained mixtures with multiple temperatures. *Arch. Ration. Mech. Anal.* 70 235-50.
- [17] Prévost, J.H., 1980. Mechanics of continuous porous media. *Int. J. Eng. Sci.* 18 (6), 787-800.
- [18] Prevost, J.H., 1982. Nonlinear transient phenomena in saturated porous media. *Comput. Methods Appl. Mech. Eng.* 30 (1), 3-18.
- [19] Simon, B., Zienkiewicz, O., Paul, D., 1984. An analytical solution for the transient response of saturated porous elastic solids. *Int. J. Numer. Anal. Methods Geomech.* 8 (4), 381-98.
- [20] Gajo, A., Mongiovi, L., 1995. An analytical solution for the transient response of saturated linear elastic porous media. *Int. J. Numer. Anal. Methods Geomech.* 19 (6), 399-413.
- [21] Ghaboussi, J., Wilson, E.L., 1972. Variational formulation of dynamics of fluid-saturated porous elastic solids. *Journal of the Engineering Mechanics Division.* 98 (4), 947-63.
- [22] Zhao, H., Indraratna, B., Ngo, T., 2021. Numerical simulation of the effect of moving loads on saturated subgrade soil. *Comput. Geotech.* 131 103930.
- [23] Liang, J., Liang, J., 2020. A user-defined element for dynamic analysis of saturated porous media in ABAQUS. *Comput. Geotech.* 126 103693.
- [24] Thigpen, L., Berryman, J.G., 1985. Mechanics of porous elastic materials containing multiphase fluid. *Int. J. Eng. Sci.* 23 (11), 1203-14.
- [25] Vardoulakis, I., Beskos, D., 1986. Dynamic behavior of nearly saturated porous media. *Mech. Mater.* 5 (1), 87-108.
- [26] Lu, Z., Fang, R., Yao, H., Dong, C., Xian, S., 2018. Dynamic responses of unsaturated half - space soil to a moving harmonic

- 1 rectangular load. *Int. J. Numer. Anal. Methods Geomech.* 42 (9), 1057-77.
- 2 [27] Jiang, Y., Ma, Q., 2022. Study on vibration isolation effect of wave impeding block in unsaturated soil under S-wave incidence.
3 *Acta Mech.* 233 (10), 4119-39.
- 4 [28] Tang, C., Lu, Z., Duan, Y., Yao, H., 2020. Dynamic responses of the pavement-unsaturated poroelastic ground system to a
5 moving traffic load. *Transp. Geotech.* 25 100404.
- 6 [29] Ye, Z., Ai, Z.Y., 2022. Elastodynamic analyses of transversely isotropic unsaturated subgrade–pavement system under moving
7 loads. *Int. J. Numer. Anal. Methods Geomech.* 46 (11), 2138-62.
- 8 [30] Li, X., Zienkiewicz, O., Xie, Y., 1990. A numerical model for immiscible two - phase fluid flow in a porous medium and its
9 time domain solution. *Int. J. Numer. Methods Eng.* 30 (6), 1195-212.
- 10 [31] Ghorbani, J., Nazem, M., Carter, J., 2016. Numerical modelling of multiphase flow in unsaturated deforming porous media.
11 *Comput. Geotech.* 71 195-206.
- 12 [32] Ghorbani, J., Airey, D.W., El-Zein, A., 2018. Numerical framework for considering the dependency of SWCCs on volume
13 changes and their hysteretic responses in modelling elasto-plastic response of unsaturated soils. *Comput. Methods Appl. Mech. Eng.*
14 336 80-110.
- 15 [33] Ghorbani, J., Airey, D.W., Carter, J.P., Nazem, M., 2021. Unsaturated soil dynamics: Finite element solution including stress-
16 induced anisotropy. *Comput. Geotech.* 133 104062.
- 17 [34] Wang, Y.D., Keshavarzi, B., Kim, Y.R., 2018. Fatigue performance prediction of asphalt pavements with FlexPAVETM, the
18 S-VECD model, and DR failure criterion. *Transp. Res. Rec.* 2672 (40), 217-27.
- 19 [35] Wang, Y.D., Keshavarzi, B., Kim, Y.R., 2018. Fatigue performance analysis of pavements with RAP using viscoelastic
20 continuum damage theory. *KSCE J. Civ. Eng.* 22 2118-25.
- 21 [36] Yang, Y.B., Hung, H.H., 2001. A 2.5 D finite/infinite element approach for modelling visco - elastic bodies subjected to
22 moving loads. *Int. J. Numer. Methods Eng.* 51 (11), 1317-36.
- 23 [37] Galvín, P., François, S., Schevenels, M., Bongini, E., Degrande, G., Lombaert, G., 2010. A 2.5 D coupled FE-BE model for
24 the prediction of railway induced vibrations. *Soil Dyn. Earthquake Eng.* 30 (12), 1500-12.
- 25 [38] Gao, G.-Y., Chen, Q., He, J., Liu, F., 2012. Investigation of ground vibration due to trains moving on saturated multi-layered
26 ground by 2.5 D finite element method. *Soil Dyn. Earthquake Eng.* 40 87-98.
- 27 [39] Charoenwong, C., Connolly, D.P., Costa, P.A., Galvín, P., Romero, A., 2024. The effect of ballast moisture content and fouling
28 index on railway track settlement. *Transp. Geotech.* 45 101193.
- 29 [40] Liu, P., Wang, D., Hu, J., Oeser, M. SAFEM-Software with graphical user interface for fast and accurate finite element analysis
30 of asphalt pavements: ASTM International, 2016.
- 31 [41] Liu, P., Wang, D., Otto, F., Hu, J., Oeser, M., 2018. Application of semi-analytical finite element method to evaluate asphalt
32 pavement bearing capacity. *Int. J. Pavement Eng.* 19 (6), 479-88.
- 33 [42] Shen, K., Wang, H., Zhang, H., Tong, J., Chen, X., 2022. SAPAVE: an improved semi-analytical FE program for dynamic
34 viscoelastic analysis of asphalt pavement. *Int. J. Pavement Eng.* 23 (9), 3024-35.
- 35 [43] Cao, Y., Xia, H., Lombaert, G., 2010. Solution of moving-load-induced soil vibrations based on the Betti–Rayleigh Dynamic
36 Reciprocal Theorem. *Soil Dyn. Earthquake Eng.* 30 (6), 470-80.
- 37 [44] Krenk, S., Kellezi, L., Nielsen, S.R., Kirkegaard, P.H. Finite elements and transmitting boundary conditions for moving loads.
38 *Finite Elements and Transmitting Boundary Conditions for Moving Loads: CRC Press/Balkema*, 1999. p. 447-52.
- 39 [45] Koh, C., Ong, J., Chua, D., Feng, J., 2003. Moving element method for train - track dynamics. *Int. J. Numer. Methods Eng.* 56
40 (11), 1549-67.
- 41 [46] Ang, K.K., Dai, J., 2013. Response analysis of high-speed rail system accounting for abrupt change of foundation stiffness. *J.*
42 *Sound Vib.* 332 (12), 2954-70.
- 43 [47] Tran, M.T., Ang, K.K., Luong, V.H., 2014. Vertical dynamic response of non-uniform motion of high-speed rails. *J. Sound*
44 *Vib.* 333 (21), 5427-42.

- 1 [48] Liu, B., Su, Q., Liu, T., Li, T., 2017. Dynamic response of water saturated subgrade surface layer under high speed train using
2 moving element method. *Journal of Vibroengineering*. 19 (5), 3720-36.
- 3 [49] Cao, C., LI, C., LI, H., 2014. Dynamic response of pavement plate - saturated
4 elastic foundation under moving loads. *J. Xi'an Univ. of Arch. & Tech. (Natural Science Edition)*. 46 (2), 7.
- 5 [50] Murad, M.A., Loula, A.F., 1994. On stability and convergence of finite element approximations of Biot's consolidation problem.
6 *Int. J. Numer. Methods Eng.* 37 (4), 645-67.
- 7 [51] Li, W., Wei, C., 2018. Stabilized low - order finite elements for strongly coupled poromechanical problems. *Int. J. Numer.*
8 *Methods Eng.* 115 (5), 531-48.
- 9 [52] Bishop, A.W., Blight, G., 1963. Some aspects of effective stress in saturated and partly saturated soils. *Geotechnique*. 13 (3),
10 177-97.
- 11 [53] Tuncay, K., Corapcioglu, M., 1997. Wave propagation in poroelastic media saturated by two fluids.
- 12 [54] Van Genuchten, M.T., 1980. A closed - form equation for predicting the hydraulic conductivity of unsaturated soils. *Soil Sci.*
13 *Soc. Am. J.* 44 (5), 892-8.
- 14 [55] Chung, J., Hulbert, G., 1993. A time integration algorithm for structural dynamics with improved numerical dissipation: the
15 generalized- α method.
- 16 [56] Newmark, N.M., 1959. A method of computation for structural dynamics. *Journal of the engineering mechanics division*. 85
17 (3), 67-94.
- 18 [57] Erlicher, S., Bonaventura, L., Bursi, O.S., 2002. The analysis of the generalized- α method for non-linear dynamic problems.
19 *Comput. Mech.* 28 (2), 83-104.
- 20 [58] Kontoe, S., Zdravkovic, L., Potts, D.M., 2008. An assessment of time integration schemes for dynamic geotechnical problems.
21 *Comput. Geotech.* 35 (2), 253-64.
- 22 [59] Simon, B., Wu, J.S., Zienkiewicz, O., Paul, D., 1986. Evaluation of $u - w$ and $u - \pi$ finite element methods for the dynamic
23 response of saturated porous media using one - dimensional models. *Int. J. Numer. Anal. Methods Geomech.* 10 (5), 461-82.
- 24 [60] Li, P., Schanz, M., 2011. Wave propagation in a 1-D partially saturated poroelastic column. *Geophys. J. Int.* 184 (3), 1341-53.
- 25 [61] Brooks, R.H. Hydraulic properties of porous media: Colorado State University, 1965.
- 26 [62] Theodorakopoulos, D., 2003. Dynamic analysis of a poroelastic half-plane soil medium under moving loads. *Soil Dyn.*
27 *Earthquake Eng.* 23 (7), 521-33.
- 28 [63] Lo, W.C., Sposito, G., Majer, E., 2005. Wave propagation through elastic porous media containing two immiscible fluids.
29 *Water Resour. Res.* 41 (2).
- 30 [64] Wu, J., Wang, K., El Naggar, M.H., 2019. Half-space dynamic soil model excited by known longitudinal vibration of a defective
31 pile. *Comput. Geotech.* 112 403-12.
- 32 [65] Steeb, H., Kurzeja, P.S., Schmalholz, S.M., 2014. Wave propagation in unsaturated porous media. *Acta Mech.* 225 2435-48.
- 33 [66] Wang, Y., Gao, G., Yang, J., Song, J., 2015. The influence of the degree of saturation on dynamic response of a cylindrical
34 lined cavity in a nearly saturated medium. *Soil Dyn. Earthquake Eng.* 71 27-30.
- 35 [67] Zhang, M., Wang, X., Yang, G., Xie, L., 2014. Solution of dynamic Green' s function for unsaturated soil under internal
36 excitation. *Soil Dyn. Earthquake Eng.* 64 63-84.
- 37 [68] Cui, X., Li, X., Hao, J., Wang, Y., Bao, Z., Du, Y., Zhou, J., 2022. Dynamic response of unsaturated poroelastic ground
38 underlying uneven pavement subjected to vehicle load. *Soil Dyn. Earthquake Eng.* 156 107164.
- 39